In this study, when the plaque thickness remained constant, expansive remodeling led to a greater concentration of stress than did constrictive remodeling. Expansive remodeling is frequently observed as a compensatory process for an increase in plaque thickness. In such a case, stress attenuation by the increase in plaque thickness is canceled by expansion in vessel diameter, which consequently maintains or enhances stress value on the plaque surface. Therefore, the present results may be consistent with the findings of previous reports (9–12) showing that unstable plaques are usually associated with expansive remodeling.

Subintimal plaque structure and stress. The significant impact of decreases in fibrous cap thickness on stress concentration within plaques has been widely shown in various studies using postmortem pathological analyses and intravascular imaging modalities (4,13–17). Our findings showed that the stress on a fibrous cap was dramatically increased when its thickness was <80 μm. This value of 80 μm actually depends on the vessel diameter. The range of cap thickness of 60 to 100 μm corresponds to vessel diameters of 2.5 to 4mm. Previous empirical cross-sectional studies have shown that a fibrous cap thickness of less than 65 to 150 μm is critical in terms of the risk of plaque rupture (15,16,25–27). Therefore, the critical thickness of fibrous caps in terms of plaque rupture might be similar in both the cross-sectional and the longitudinal direction. However, the present study using longitudinal IVUS showed that the critical thickness of a fibrous cap leading to rupture varies greatly because of differences in the distribution of surrounding calcifications, even with the same vessel diameter. The involvement of calcification, and variabilities in plaque thickness and shape, may account for inconsistencies regarding the critical thickness reported in several previous studies, which has been shown to vary between 65 and 150 μm (15,16,25–27). The effect of vessel size would also account for a range of the critical thickness varying from 60 to 100 μm as noted above. Furthermore, our results suggest that the measurement of fibrous cap thickness alone is inadequate for identifying plaques vulnerable to rupture.

The presence of a lipid core was also an important factor in stress concentration, according to our study of the longitudinal vessel axis. However, increasing the size of a lipid core did not affect the surface stress of plaques, provided the thickness of the fibrous cap remained constant. These studies, as well as our own, may support the findings of previous reports showing that plaque rupture can be observed in the region of a fibrous cap, even in the presence of a very small lipid core (18,25,28).

Calcification is commonly found in atherosclerosis, but the role of calcification in plaque rupture is still unknown. Some studies indicate beneficial effects in stabilizing plaque (19,23,29), whereas some suggest its worsening effects to plaque vulnerability (30–34). In our study, calcification significantly affected the stress on fibrous caps that were either adjacent to or at a slight distance from calcifications. The exact mechanisms of the attenuation of stress by surface calcification are unclear.

Clinical implications. Although a variety of factors may participate in the process of plaque rupture, including hemodynamic shear stress (20), turbulent pressure fluctuations (35), transient compression (36), sudden increase in intraluminal pressure (37), rupture of the vaso vasorum (38), material fatigue (4,18,39), and cellular inflammatory reactions (3,4,22,40), this study suggests that assessment of stress concentration within a plaque along the longitudinal axis of a vessel is also important for identifying vulnerable plaques. Therefore, this approach may help identify vulnerable plaques or even help predict the point of future rupture.

Study limitations. To simplify the present finite element analysis, the materials were assumed to be isotropic, incompressible, and uniform solids. By assuming that plaques, lipids, calcium, and normal arterial walls could each be characterized by a single set of structural parameters, spatial and interspecimen variations within a particular component were not considered here. However, the assumptions used in this study have been widely accepted as allowable for the assessment of the biomechanical properties of atherosclerotic lesions (13,23). The model used in this study was a linear one, although almost all of the biomaterials have nonlinear properties. Actually, there are only limited data available with regard to the nonlinear biomechanical behavior of atherosclerotic lesions. Furthermore, in the present study, we examined factors affecting relative stress values and not exact absolute stress magnitudes.

In this study, we used an axisymmetric model, although clinical plaques are not always axisymmetric in geometry. The purpose of this study was limited to assess the longitudinal determinants of plaque vulnerability, but not cross-sectional determinants, which were already clarified in the numerous previous studies. Therefore, the axisymmetric model was used to exclude the cross-sectional determinants of stress distribution within plaques.

It was also assumed in this study that there were no shear stresses, torques, time-varying forces, or flow-related forces; only static blood pressure was considered to be acting on the lesion in the models. It has been documented that the effect of fluid shear stress is insignificant when compared with the effect of tensile wall stresses (19) as a direct component in plaque fracture dynamics. The estimation of stresses induced by static pressure load alone has already shown its usefulness in identifying stress concentration in human lesions (23), because the location of stress concentration does not significantly differ between the single static pressure model and the complex dynamic pressure model.

Reprint requests and correspondence: Dr. Takafumi Hiro, Department of Molecular Cardiovascular Biology, Yamaguchi University Graduate School of Medicine, 1-1-1 Minami Kogushi, Ube, Yamaguchi, 755-8505, Japan. E-mail: thiro@yamaguchi-u.ac.jp.

REFERENCES

1. Levin DC, Fallon JT. Significance of the angiographic morphology of localized coronary stenosis: histopathologic correlations. Circulation 1982;66:316–20.
2. Davies MJ, Thomas A. Thrombosis and acute coronary artery lesions in sudden cardiac ischemic death. N Engl J Med 1984;310:1137–40.
3. Shah PK. Mechanism of plaque vulnerability and rupture. J Am Coll Cardiol 2003;41 Suppl 1:15–22.
4. Falk E, Shah PK, Fuster V. Coronary plaque disruption. Circulation 1995;92:657–71.
5. Nobuyoshi M, Tanaka M, Nosaka H, et al. Progression of coronary atherosclerosis: is coronary spasm related to progression? J Am Coll Cardiol 1991;18:904–10.
6. Giroud D, Li JM, Urban P, Meier B, Rutishauer W. Relation of the site of acute myocardial infarction to the most severe coronary arterial stenosis at prior angiography. Am J Cardiol 1992;69:729–32.
7. Ambrose JA, Tannenbaum MA, Alexopoulos D, et al. Angiographic progression of coronary artery disease and the development of myocardial infarction. J Am Coll Cardiol 1988;12:56–62.
8. Little WC, Constantinescu M, Applegate RJ, et al. Can coronary angiography predict the site of a subsequent myocardial infarction in patients with mild-to-moderate coronary artery disease? Circulation 1988;78:1157–66.
9. Schoenhagen P, Ziada KM, Kapadia SR, Crowe TD, Nissen SE, Tuzcu EM. Extent and direction of arterial remodeling in stable versus unstable coronary syndromes: an intravascular ultrasound study. Circulation 2000;101:598–603.
10. Birgelen CV, Klinkhart W, Mintz GS, et al. Plaque distribution and vascular remodeling of ruptured and nonruptured coronary plaques in the same vessel: an intravascular ultrasound study in vivo. J Am Coll Cardiol 2001;37:1864–70.
11. Shoenhagen P, Ziada KM, Vince DG, Nissen SE, Tuzcu EM. Arterial remodeling and coronary artery disease: the concept of "dilated" versus "obstructive" coronary atherosclerosis. J Am Coll Cardiol 2001;38:297–306.
12. Smits PC, Pasterkamp KR, deJaegere PPT, Feyter PJ, Borst C. Angioscopic complex lesions are predominantly compensatory enlarged. Cardiovasc Res 1999;41:458–64.
13. Loree HM, Kamm RD, Stringfellow RG, Lee RT. Effects of fibrous cap thickness on peak circumferential stress in model atherosclerotic vessels. Circ Res 1992;71:850–8.
14. Nissen SE, Yock P. Intravascular ultrasound: novel pathophysiological insights and current clinical applications. Circulation 2001;103:604–16.
15. Maseri A, Fuster V. Is there a vulnerable plaque? Circulation 2003; 107:2068–71.
16. Virmani R, Kolodgie FD, Burke AP, Farb A, Schwartz SM. Lessons from sudden coronary death: a comprehensive morphological classification scheme for atherosclerotic lesions. Arterioscler Thromb Vasc Biol 2000;20:1262–75.
17. Davies MJ, Richardson PD, Woolf N, et al. Risk of thrombosis in human atherosclerotic plaques: role of extracellular lipid, macrophage, and smooth muscle cell content. Br Heart J 1993;69:377–81.
18. Richardson PD, Davies MJ, Born GV. Influence of plaque configuration and stress distribution on fissuring of coronary atherosclerotic plaques. Lancet 1989;2:941–4.
19. Huang H, Virmani R, Younis H, Burke AP, Kamm RD, Lee RT. The impact of calcification on the biomechanical stability of atherosclerotic plaques. Circulation 2001;103:1051–6.
20. Gertz SD, Roberts WC. Hemodynamic shear force in rupture of coronary arterial atherosclerotic plaques. Am J Cardiol 1990;66: 1368–72.
21. Hodgson JM, Reddy KG, Suneja R, Nair RN, Lesnefsky EJ, Sheehan HM. Intracoronary ultrasound imaging: correlation of plaque morphology with angiography, clinical syndrome and procedural results in patients undergoing coronary angiography. J Am Coll Cardiol 1993;21:35–44.
22. Lendon CL, Davies MJ, Born GV, Richardson PD. Atherosclerotic plaque caps are locally weakened when macrophage density is increased. Atherosclerosis 1991;87:87–90.
23. Cheng GC, Loree HM, Kamm RD, Fishbein MC, Lee RT. Distribution of circumferential stress in ruptured and stable atherosclerotic lesions: a structural analysis with histopathological correlation. Circulation 1993;87:1179–87.
24. Lee RT, Loree HM, Cheng GC, Lieberman EH, Jaramillo N, Schoen FJ. Computational structural analysis based on intravascular ultrasound imaging before in vitro angiography: prediction of plaque fracture locations. J Am Coll Cardiol 1993;21:777–82.
25. Ge J, Chirillo F, Schwedtmann J, et al. Screening of ruptured plaques in patients with coronary artery disease by intravascular ultrasound. Heart 1999;81:621–7.
26. Burke AP, Farb A, Malcom GT, Liang Y, Smialek J, Virmani R. Coronary risk factors and plaque morphology in men with coronary disease who died suddenly. N Engl J Med 1997;336:1276–82.
27. MacNeill BD, Lowe HC, Takano M, Fuster V, Jang IK. Intravascular modalities for detection of vulnerable plaque: current status. Arterioscler Thromb Vasc Biol 2003;23:1333–42.
28. Mann JM, Davies MJ. Vulnerable plaque: relation of characteristics to degree of stenosis in human coronary arteries. Circulation 1996;94: 928–31.
29. Alderman EL, Corley SD, Fisher LD, et al. Five-year angiographic follow-up of factors associated with progression of coronary artery disease in the Coronary Artery Surgery Study (CASS). J Am Coll Cardiol 1993;22:1141–54.
30. Raggi P, Callister TQ, Cooil B, et al. Identification of patients at increased risk of first unheralded acute myocardial infarction by electron-beam computed tomography. Circulation 2000;101:850–5.
31. Arad Y, Spadaro LA, Goodman K, Newstein D, Guerci AD. Prediction of coronary events with electron beam computed tomography. J Am Coll Cardiol 2000;36:1253–60.
32. Taylor AJ, Burke AP, O'Malley PG, et al. A comparison of the Framingham risk index, coronary artery calcification, and culprit morphology in sudden cardiac death. Circulation 2000;101:1243–8.
33. Schmermund A, Erbel R. Unstable coronary plaque and its relation to coronary calcium. Circulation 2001;104:1682–7.
34. Mintz GS, Pichard AD, Popma JJ, et al. Determinants and correlates of target lesion calcium in coronary artery disease: a clinical, angiographic and intravascular ultrasound study. J Am Coll Cardiol 1997; 29:268–74.
35. Loree HM, Kamm RD, Atkinson CM, Lee RT. Turbulent pressure fluctuations on surface of model vascular stenosis. Am J Physiol 1991;261:H644–50.
36. Binns RL, Ku DN. Effect of stenosis on wall motion: a possible mechanism of stroke and transient ischemic attack. Arteriosclerosis 1989;9:842–7.
37. Muller JE, Tofler GH, Stone PH. Circadian variation and triggers of onset of acute cardiovascular disease. Circulation 1989;79:733–43.
38. Barger AC, Beeuwkes R, Lainey LL, Silverman KJ. Hypothesis: vasa vasorum and neovascularization of human coronary arteries. A possible role in the pathophysiology of atherosclerosis. N Engl J Med 1984; 310:175–7.
39. MacIsaac AI, Thomas JD, Topol EJ. Toward the quiescent coronary plaque. J Am Coll Cardiol 1993;22:1228–41.
40. Davies MJ. Stability and instability: two faces of coronary atherosclerosis. Circulation 1996;94:2013–20.

nature medicine

Regression of abdominal aortic aneurysm by inhibition of c-Jun N-terminal kinase

Koichi Yoshimura[1], Hiroki Aoki[1], Yasuhiro Ikeda[1], Kozo Fujii[1], Norio Akiyama[2], Akira Furutani[2], Yoshinobu Hoshii[3], Nobuyuki Tanaka[4], Romeo Ricci[5], Tokuhiro Ishihara[3], Kensuke Esato[2], Kimikazu Hamano[2] & Masunori Matsuzaki[1,6]

Abdominal aortic aneurysm (AAA) is a common disease among elderly people that, when surgical treatment is inapplicable, results in progressive expansion and rupture of the aorta with high mortality. Although nonsurgical treatment for AAA is much awaited, few options are available because its molecular pathogenesis remains elusive. Here, we identify JNK as a proximal signaling molecule in the pathogenesis of AAA. Human AAA tissue showed a high level of phosphorylated JNK. We show that JNK programs a gene expression pattern in different cell types that cooperatively enhances the degradation of the extracellular matrix while suppressing biosynthetic enzymes of the extracellular matrix. Selective inhibition of JNK *in vivo* not only prevented the development of AAA but also caused regression of established AAA in two mouse models. Thus, JNK promotes abnormal extracellular matrix metabolism in the tissue of AAA and may represent a therapeutic target.

AAA affects 6–9% of men over the age of 65 years and is the tenth leading cause of death in men over the age of 55 years in the United States[1]. When surgical treatment is inapplicable, AAA progresses to rupture with a high mortality, as an effective nonsurgical therapy is currently not available. Because many cases of AAA are at a high risk for rupture at the time of initial diagnosis, and the aortic diameter is the major predictor of rupture, a nonsurgical therapy that reduces AAA diameter would have a considerable impact on the current therapeutic strategy to reduce the risk of rupture[2].

AAA is characterized by atherosclerotic changes with chronic inflammation of aortic walls where resident vascular smooth muscle cells (VSMCs) and infiltrating macrophages release matrix metalloproteinases (MMPs), particularly MMP-9 and MMP-2 (refs. 3–5). These MMPs cause the loss of crucial extracellular matrix (ECM) components including collagen and elastin, whereas unknown mechanisms may suppress normal ECM biosynthesis by VSMCs[6–9], leading to development of AAA. Pharmacological inhibition of MMPs cause a slower expansion rate of AAA in animal models[7,10–12] and in early clinical trials[13,14]. Effective regression of AAA by nonsurgical therapy, however, has not been reported, and AAA has been considered an irreversible destructive process. Notably, it has been suspected that inhibition of MMPs[7] or endovascular seeding of VSMCs[15] may sometimes, but not always, cause regression of experimental AAA. Moreover, successful endovascular stent grafting results in the shrinkage (regression) of AAA diameter in some people[16], suggesting that the diseased aorta has the potential to regress if exacerbating factors are eliminated and/or the tissue repair is reinforced.

Various stimuli have been linked to chronic inflammation observed in AAA, including mechanical stress, oxidative stress, angiotensin II (AngII), tumor necrosis factor (TNF)-α, interleukin (IL)-1β, IL-6 and interferon (IFN)-γ (reviewed in ref. 1). Most, if not all, of these stimuli activate c-Jun N-terminal kinase (JNK, also known as stress-activated protein kinase) in VSMCs, which synthesize ECM[1] and secrete MMPs[4,17], and macrophages, which secrete proinflammatory cytokines and MMPs[1]. Because JNK is thought to be involved in a number of cellular stress responses[18], it may have an important role in AAA. No causal relationship, however, has been reported between JNK and AAA thus far.

To obtain insight into the role of JNK in AAA, we screened for JNK-dependent genes in VSMCs. Here, we report the essential role of JNK in abnormal metabolism of ECM and disease progression of AAA. Notably, pharmacological inhibition of JNK restored the architecture of aortic tissue and caused regression of established AAA in mice.

RESULTS

JNK-dependent gene expression pattern in VSMCs

We performed DNA microarray analyses using rat aortic VSMCs in culture to screen for genes regulated by JNK, utilizing both gain-of-function and loss-of-function strategies (**Supplementary Fig. 1** online). We used adenoviral vectors to coexpress constitutively active MKK7 (caMKK7) and wild-type JNK1 to achieve gain of function of the JNK pathway. We achieved loss of function of the JNK pathway by expressing dominant negative JNK1 (dnJNK1), which sequesters upstream kinases, thereby blocking the activation of all JNK isoforms.

[1]Department of Molecular Cardiovascular Biology, [2]Department of Cardiovascular Surgery, [3]First Department of Pathology and [4]Department of Radiology, Yamaguchi University School of Medicine, 1-1-1 Minami Kogushi, Ube, Yamaguchi 755-8505, Japan. [5]ETH Hönggerberg, Institute of Cell Biology, CH-8093 Zurich, Switzerland. [6]Department of Cardiovascular Medicine Yamaguchi University School of Medicine 1-1-1 Minami Kogushi, Ube, Yamaguchi 755-8505, Japan. Correspondence should be addressed to H.A. (haoki@yamaguchi-u.ac.jp).

Received 19 April; accepted 1 November; published online 27 November 2005; doi:10.1038/nm1335

Table 1 JNK-regulated genes in rat aortic VSMCs

Accession number	Description	R_{caVKK7}	P_{caVKK7}	R_{dnJNK}	P_{dnJNK}	JNK dependence Index
JNK-induced genes (top 20)						
D00403	Interleukin 1 alpha	2.9	0.030	2.8	0.043	3.892
S62933	TrkC	2.7	0.250	3.2	0.081	3.533
U10697	Similar to liver carboxylesterase	2.6	0.010	2.9	0.001	3.492
M35077	Dopamine receptor 1A	2.5	0.050	2.7	0.000	3.407
U16359	Inducible nitric oxide synthase	2.4	0.090	2.5	0.102	3.327
AA875123	EST	2.5	0.080	2.9	0.002	3.301
AA799492	Proteasome subunit, alpha	2.5	0.760	2.9	0.307	3.301
AA685217	EST, similar to Galnt6	2.7	0.010	2.3	0.006	3.021
L28114	Aquaporin 3	2.4	0.200	2.2	0.004	2.984
AA799663	EST, similar to T10	3.4	0.001	2.4	0.313	2.938
U24441	Matrix metallopeptidase 9	2.2	0.001	2.5	0.102	2.931
U79568	Na channel, voltage-gated	2.2	0.000	2.1	0.000	2.903
AF064856	7acomp protein	2.2	0.110	2.1	0.086	2.903
X60328	Epoxide hydrolase 2, cytoplasmic	2.4	0.020	3.8	0.000	2.839
M94548	CYP4F2	2.0	0.080	2.2	0.233	2.703
AI639322	EST	1.9	0.140	1.9	0.023	2.687
U32372	Sulfotransferase family 1D	2.1	0.480	2.7	0.000	2.660
AA946503	Lipocalin 2	2.7	0.003	2.1	0.463	2.660
AJ002259	Short stature homeobox 2	2.1	0.500	1.9	0.070	2.562
X13804	Neurofilament, heavy polypeptide	1.9	0.020	2.3	0.112	2.464
Genes encoding biosynthetic enzymes for collagen and elastin						
L25331	Lysyl hydroxylase	0.2	0.920	0.5	1.000	0.215
AI102814	Lysyl oxidase	0.4	0.990	0.3	0.937	0.375
X78949	Prolyl 4-hydroxylase	0.7	1.000	0.4	1.000	0.461

The 20 genes with highest JNK dependence Index and the genes encoding biosynthetic enzymes for collagen and elastin are shown. Positive values of R_{dnJNK} indicate the suppression of these genes by dnJNK. *P* values for the caVKK7 set (P_{caVKK7}) and the dnJNK set (P_{dnJNK}) were interpreted as follows: 0–0.0025, increase; 0.0025–0.003, marginal increase; 0.003–0.997, no change; 0.997–0.9975, marginal decrease; 0.9975–1.0, decrease.

As oxidative stress has an important role in vascular diseases[19], we used H_2O_2 to activate the JNK pathway[20]. We defined JNK-regulated genes as those downregulated after inhibition of JNK in the presence of H_2O_2 and upregulated after activation of JNK (JNK-induced genes) or vice versa (JNK-suppressed genes), and ranked them using the JNK Dependence Index (**Supplementary Fig. 2** online). The entire list of JNK-regulated genes is presented in the **Supplementary Table** online. Several genes with a high JNK Dependence Index encode proteins thought to be involved in proinflammatory signaling, including those encoding IL-1α, TrkC, inducible nitric oxide synthase and MMP-9 (**Table 1**). In addition, lipocalin-2, which binds to and maintains the activity of MMP-9 (ref. 21), also had a high JNK Dependence Index.

Impaired biosynthesis of the ECM has been proposed as a mechanism of pathogenesis of AAA[7–9,22]. Our DNA microarray data showed that JNK downregulates the gene expression of crucial ECM biosynthetic enzymes, including lysyl hydroxylase (encoded by *Plod1*; essential for the stability of collagen fibers), lysyl oxidase (encoded by *Lox*; responsible for the cross-linking and deposition of collagen and elastin fibers) and prolyl 4-hydroxylase (encoded by *P4ha1*; the rate-limiting enzyme for collagen biosynthesis; **Table 1**). These data suggest that JNK activation may lead to activation of MMP-9 and proinflammatory signaling, which have central roles in AAA[1,3,4], and at the same time it may suppress biosynthesis and deposition of ECM that is crucial for the integrity of the aortic wall.

JNK and MMP-9 in human AAA walls

We next determined whether JNK is phosphorylated at its activation loop in human AAA tissue. We also analyzed expression of p38, ERK, MMP-2 and MMP-9, and phosphorylation of the MAP kinases in samples of aortic wall from individuals with or without AAA. Levels of both total JNK and phosphorylated JNK were markedly increased in human AAA (**Fig. 1a,b**). Although expression of p38 was elevated in AAA, expression of phosphorylated p38 was not. We observed no significant change in levels of total ERK or phosphorylated ERK in AAA (**Fig. 1a,b**). MMP-9 expression was highly elevated and MMP-2 was moderately elevated in AAA samples, as determined by gelatin zymography (**Fig. 1a,c**) and as reported previously (reviewed in ref. 19). MMP-9 expression levels showed a highly positive correlation with levels of phosphorylated JNK (**Fig. 1d**, $r = 0.76$). Levels of ERK, phosphorylated ERK, p38 and phosphorylated p38 levels were not correlated with MMP-9 expression levels (data not shown).

We examined the tissue localization of phosphorylated JNK and MMP-9 in human AAA walls. Phosphorylated JNK and MMP-9 colocalized in the adventitia and outer media (**Fig. 1e,f**). In contrast, relatively weak signals from phosphorylated JNK were scattered throughout the thickened intima of aortic tissue from a case of aortoiliac occlusive disease (AOD, **Supplementary Fig. 3** online). Most of the signal from phosphorylated JNK was localized in VSMCs in the outer media (**Fig. 1g**) and in macrophages in the adventitia (**Fig. 1h**). These results, together with the DNA microarray data, prompted us to further investigate the link between JNK activation and MMP expression in AAA.

The role of JNK in the ECM degradation pathway

Because MMP-9 and phosphorylated JNK were localized in VSMCs and macrophages in AAA, we examined the causal relationship

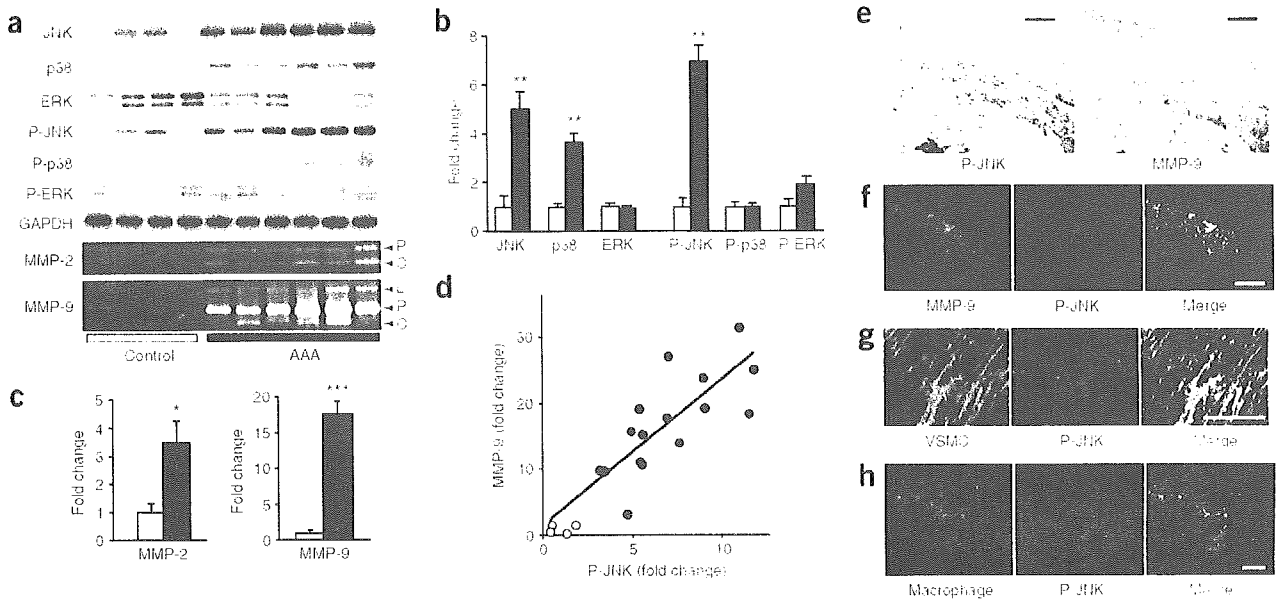

Figure 1 Expression and phosphorylation of MAP kinases and MMPs in human AAA. (**a**–**c**) Representative western blots are shown for ERK, p38 and JNK and for their phosphorylated forms (P-ERK, P-p38 and P-JNK, respectively) and gelatin zymograms for MMP-9 and MMP-2 (**a**) with quantitative analyses (**b**,**c**). P, proforms of MMPs; C, cleaved forms of MMPs; L, lipocalin-2–MMP-9 complex. GAPDH signal served as internal control of protein loading. Data were obtained from four individuals without AAA (control, open columns) and 17 individuals with AAA (closed columns), and expressed as fold changes compared with control. $^{*}P < 0.05$, $^{**}P < 0.01$, $^{***}P < 0.001$, compared with control. (**d**) Linear correlation ($r = 0.76$) between the levels of P-JNK and MMP-9. Open circles, control; closed circles, AAA. (**e**) The localization of P-JNK and MMP-9 are shown by immunohistochemistry in serial sections of human AAA, as indicated by red staining. Lumenal surface is oriented to the top. Scale bars, 500 μm. (**f**–**h**) Images of double immunofluorescence staining are shown for P-JNK (red) with MMP-9 (**f**, in green), with VSMCs (**g**, α-smooth muscle actin in green) and with macrophages (**h**, CD68 in green). Yellow in merged images indicates overlapping localization of the red and green signals. Scale bars, 200 μm.

between JNK activity and MMP secretion in rat aortic VSMCs and THP-1, a human monocyte-macrophage cell line. We used TNF-α as a stimulus because it is thought to be involved in the pathogenesis of AAA[1] and induces higher levels of MMP-9 secretion than H_2O_2 in these cells (data not shown).

Rat VSMCs in culture secreted MMP-9 in response to TNF-α, which was abrogated by JNK inhibition with SP600125, a specific inhibitor of JNK (**Fig. 2a**). Inhibition of JNK also suppressed the secretion of MMP-2 (**Fig. 2b**), which is the major MMP secreted from VSMCs and which participates in the pathogenesis of AAA[1]. Recently,

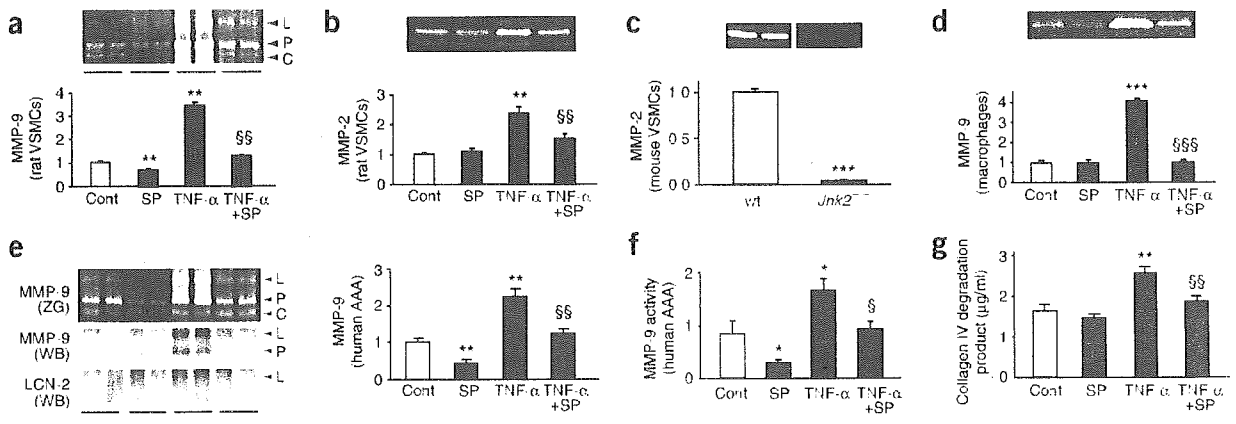

Figure 2 The role of JNK in secretion of MMPs. (**a**–**e**) Secretion of MMP-9 or MMP-2 from VSMCs, THP-1 macrophages or human AAA *ex vivo* culture was examined by gelatin zymography of the conditioned media. Representative zymograms are shown with quantitative analyses. Gelatin zymography (ZG) detected three bands corresponding the size of proform (P), cleaved form (C) and lipocalin-2 complex (L) of MMP-9 as confirmed by western blotting (WB) for MMP-9 and lipocalin-2 (LCN-2) in **e**. Cleaved MMP-9 is not visible by western blotting because of the weak signal. (**f**) Activity of secreted MMP-9 was analyzed in its native form. (**g**) ELISA results are shown for soluble collagen IV degradation product in the conditioned media of human AAA cultures. Data are means ± s.e.m. of five independent observations as shown by fold change compared with control (Cont) or wild-type (**c**) or by absolute concentration (**g**, μg/ml). $^{*}P < 0.05$, $^{**}P < 0.01$, $^{***}P < 0.001$, compared with control or wild-type (**c**). §$P < 0.05$, §§$P < 0.01$, §§§ $P < 0.001$, compared with TNF-α alone. SP, SP600125.

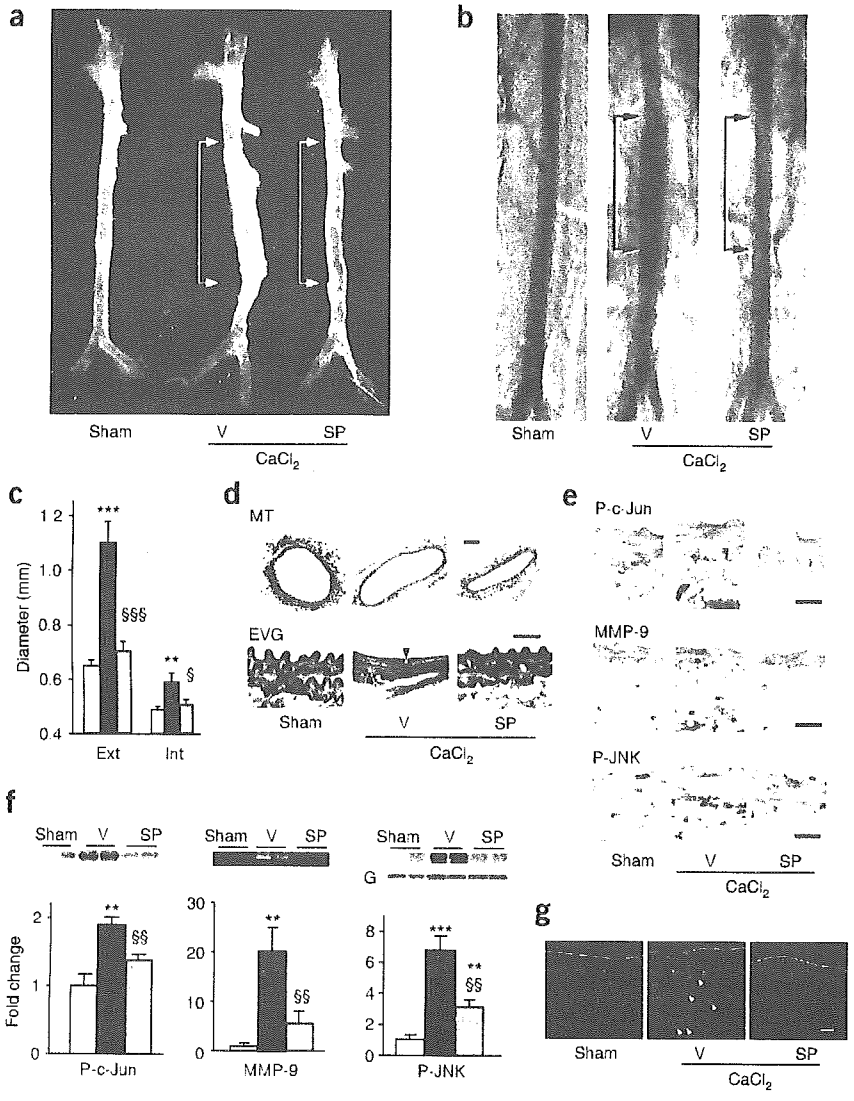

Figure 3 Prevention of the development of AAA by JNK inhibition. Aortic morphometry was performed after perfusion fixation of the aortae at the physiological perfusion pressure. (**a**) A representative photograph is shown for aortae treated with saline (Sham) or $CaCl_2$ followed by vehicle (V) or SP600125 (SP). (**b**) Representative X-ray aortograms are shown for mouse aortae treated as described in **a**. Arrows indicate the area where $CaCl_2$ was applied. (**c**) Quantitative analyses are shown for the maximal external (Ext) and internal (Int) aortic diameters. (**d**) Histological analyses were performed by Masson trichrome stain (MT) and by elastica van Gieson stain (EVG). Arrowheads indicate disrupted elastic lamella. Scale bar for MT, 100 μm; for EVG, 20 μm. (**e**,**f**) Effect of JNK inhibition is shown for phosphorylated c-Jun (P-c-Jun), MMP-9 and phosphorylated JNK (P-JNK) by immunostaining (**e**), western blotting and gelatin zymography (**f**). GAPDH signal (G) served as an internal loading control. (**g**) Immunofluorescence stainings are shown for macrophages (yellow) and nuclei (red). Macrophages are indicated by white arrowheads. The lumenal surfaces of aortic walls are outlined by white lines. Scale bar in **e** and **g**, 30 μm. White columns, sham; black columns, $CaCl_2$ + vehicle; gray columns, $CaCl_2$ + SP. Data are means ± s.e.m. from eight (**c**) and five (**f**) independent observations. $^{**}P < 0.01$, $^{***}P < 0.001$, compared with sham group. $^{§}P < 0.05$, $^{§§}P < 0.01$, $^{§§§}P < 0.001$, compared with $CaCl_2$ + vehicle group.

a crucial role for JNK2 in atherosclerosis was reported[23]. Because atherosclerosis represents the underlying vascular disease in the majority of AAA, we examined whether JNK2 is involved in secretion of MMPs from mouse VSMCs. MMP-2 was almost undetectable in the conditioned media of *Jnk2*$^{-/-}$ VSMCs, whereas it was readily detected in that of wild-type VSMCs (**Fig. 2c**). MMP-9 was barely detectable in the conditioned media of mouse VSMCs (data not shown). THP-1 cells secreted MMP-9 in response to TNF-α, which was inhibited by SP600125 (**Fig. 2d**). Adenoviral expression of dnJNK1 showed similar results, confirming the specificity of SP600125 (**Supplementary Fig. 4** online).

We next determined whether these findings were relevant to human AAA, which has complex cellular and extracellular components. Human AAA tissue in *ex vivo* culture produced a substantial amount of MMP-9, presumably induced by endogenous inflammatory signaling. SP600125 lowered the basal and TNF-α–induced secretion of MMP-9 (**Fig. 2e**). SP600125 also reduced the amount of lipocalin-2–MMP-9 complex in rat VSMCs and human AAA tissue in culture (**Fig. 2a**,**e**), consistent with the DNA microarray analyses. We also observed regulation of MMP-9 by JNK in the tissue lysate, as determined by western blotting (**Supplementary Fig. 4** online). MMP-9 secreted by AAA tissue was catalytically active, as determined by an MMP-9 assay system that detects MMP-9 activity in its native form (**Fig. 2f**). Inhibition of JNK also prevented tissue destruction induced by TNF-α, as determined by decreased levels of a soluble degradation product of collagen IV, a substrate of MMP-2 and MMP-9, in the conditioned media (**Fig. 2g**). These data indicate that JNK activity is essential for the production of MMPs that are involved in the pathogenesis of AAA[3,4] in VSMCs, macrophages and AAA tissue. The data also suggest that inhibition of JNK may be a therapeutic strategy to prevent destruction of tissue by MMPs in AAA.

Prevention of AAA development by JNK inhibition

We next asked whether JNK is involved in the pathogenesis of AAA *in vivo* using a mouse model of AAA induced by periaortic application of $CaCl_2$ (ref. 4). We chose pharmacological inhibition of JNK to address this question because of the practical relevance of a pharmacological approach in humans with AAA.

After application of saline (sham group, $n = 8$) or $CaCl_2$, we treated mice with SP600125 (SP group, $n = 8$) or vehicle (vehicle group, $n = 8$) for 10 weeks. The administration of SP600125 or vehicle did not affect the blood pressure of the mice (data not shown). Morphometric analyses of the aortae after perfusion fixation showed significant dilation of the external and internal aortic diameters in the vehicle group compared with the sham group (**Fig. 3a–c**). The dilation of the aorta was accompanied by thinning of the medial layer and

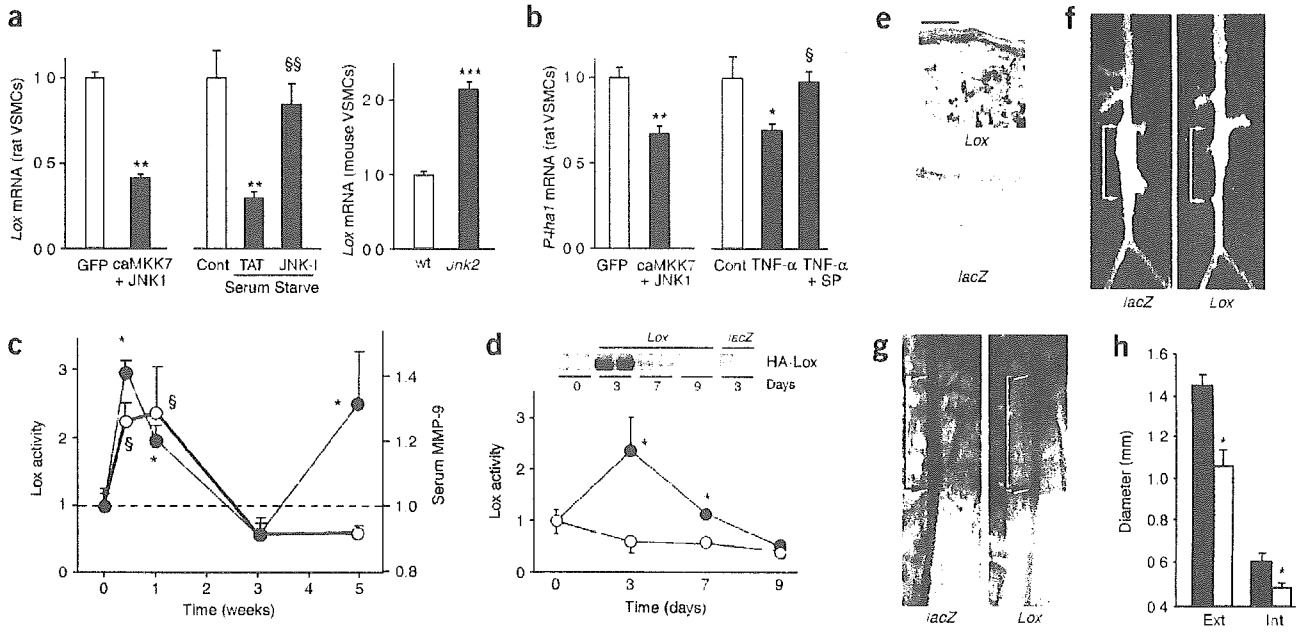

Figure 4 The role of ECM biosynthesis in AAA development. (**a**,**b**) mRNA levels of *Lox* (**a**) and *P4ha1* (**b**) were examined and normalized for *Gapdh* mRNA in VSMCs derived from rat or wild-type (wt) or *Jnk2*$^{-/-}$ mice. JNK was inhibited by a peptide inhibitor (JNK-I) or SP600125 (SP). Data are means ± s.e.m. ($n = 6$) as shown by fold change compared with Ad-GFP, control or wild-type. $^{*}P < 0.05$, $^{**}P < 0.01$, $^{***}P < 0.001$, compared with Ad-GFP, control or wild-type. §$P < 0.05$ compared with TNF-α alone, §§$P < 0.01$ compared with a control peptide (TAT). (**c**) Aortic Lox activity (open circles) and serum MMP-9 levels (filled circles) were measured at the indicated time after $CaCl_2$ treatment. Data are means ± s.e.m. ($n = 4$) compared with those before $CaCl_2$ treatment. $^{*}P < 0.05$ compared with the level of MMP-9 before $CaCl_2$ treatment, §$P < 0.05$ compared with the level of Lox activity before $CaCl_2$ treatment. (**d**,**e**) The effect of *Lox* (filled circles) or *lacZ* (open circles) gene transfer is shown by Lox assay ($n = 5$), a representative western blot (**d**) and immunohistochemistry (**e**, brown) for hemagglutinin (HA) epitope tag. Scale bar, 50 μm. (**f**–**h**) Effect of *Lox* or *lacZ* gene transfer on AAA is shown by representative photographs (**f**), aortograms (**g**) and quantification of external (Ext) and internal (Int) aortic diameters (**h**). Black columns, Ad-*lacZ*-treated ($n = 5$); gray columns, Ad-Lox-treated ($n = 8$) groups, respectively. Data are means ± s.e.m. $^{*}P < 0.05$ compared with Ad-*lacZ* group.

disruption of the elastic lamellae (**Fig. 3d**), which showed flattened morphology instead of the wavy morphology observed in normal aortae. These features are hallmarks of human AAA. Treatment of mice with SP600125 completely abrogated dilation of the aorta induced by $CaCl_2$ (**Fig. 3a–c**) and largely prevented thinning of the media and disruption of the elastic lamellae (**Fig. 3d**). SP600125 reduced the levels of phosphorylated c-Jun, the best-characterized substrate of JNK, MMP-9 and phosphorylated JNK (**Fig. 3e,f**). In addition, SP600125 reduced macrophage infiltration in the periaortic tissue (**Fig. 3g**), suggesting that chronic inhibition of JNK abrogates proinflammatory signaling[24] in AAA. These findings show that inhibition of JNK is an effective therapeutic approach to prevent tissue degradation in AAA.

The role of JNK in the biosynthesis of ECM

Based on our DNA microarray analyses (**Table 1**), we next determined whether JNK participated in the regulation of ECM biosynthesis. We also investigated the role of ECM biosynthesis in AAA. We performed gene-specific analyses for *Lox* and *P4ha1* to validate the DNA microarray data. Specific activation of JNK by adenoviral vectors encoding caMKK7 (Ad-caMkk7) and JNK1 (Ad-Jnk1) suppressed *Lox* mRNA levels (**Fig. 4a**). As TNF-α caused acute induction of *Lox* mRNA in a JNK-independent manner (H.A., unpublished observation), we applied cellular stress to VSMCs by long-term serum starvation to activate JNK. We used D-JNK-I-1 (**Supplementary Fig. 1** online), a cell-permeable specific inhibitor of JNK that achieves long-term suppression of JNK activity[25]. Serum starvation for 6 d caused a decrease in *Lox* mRNA, which was largely prevented by D-JNK-I-1 (**Fig. 4a**). As we found that JNK2 is essential for MMP-2 expression, we examined whether JNK2 was involved also in expression of *Lox*. *Jnk2*$^{-/-}$ VSMCs showed 2.1-fold higher expression of *Lox* mRNA compared with VSMCs from wild-type mice (**Fig. 4a**). *P4ha1* also showed JNK-dependent suppression (**Fig. 4b**).

We focused on the role of Lox in AAA *in vivo*, because reduced Lox activity is thought to be involved in the pathogenesis of AAA[6–8,22]. We measured both the enzymatic activity of Lox in aortae and serum MMP-9 levels after $CaCl_2$ treatment (**Fig. 4c**). Both Lox activity and serum MMP-9 levels increased early after $CaCl_2$ treatment, and decreased to below basal levels at 3 weeks. The acute increase in Lox activity may be the result of proinflammatory cytokines such as TNF-α, which induces *Lox* mRNA expression in a JNK-independent manner in VSMCs (H.A., unpublished observation). Notably, serum MMP-9 levels increased again 5 weeks after $CaCl_2$ treatment, whereas Lox activity stayed below basal levels, suggesting an imbalance between tissue degradation and repair activities in chronic AAA.

As *in vivo* evidence has been lacking as to whether reduced Lox activity has a causal role in AAA development, we performed *Lox* gene transfer *in vivo* 3 weeks after $CaCl_2$ treatment, when endogenous Lox activity was suppressed and MMP-9 levels started to rise (**Fig. 4c**). Western blotting, Lox activity assay (**Fig. 4d**) and immunostaining (**Fig. 4e**) confirmed expression of exogenous Lox in mouse aortic tissue. Aortic morphometry showed partial prevention of the development of $CaCl_2$-induced AAA by Ad-Lox ($n = 8$), but not by Ad-*lacZ* ($n = 5$; **Fig. 4f–h**), indicating that transient enhancement of Lox

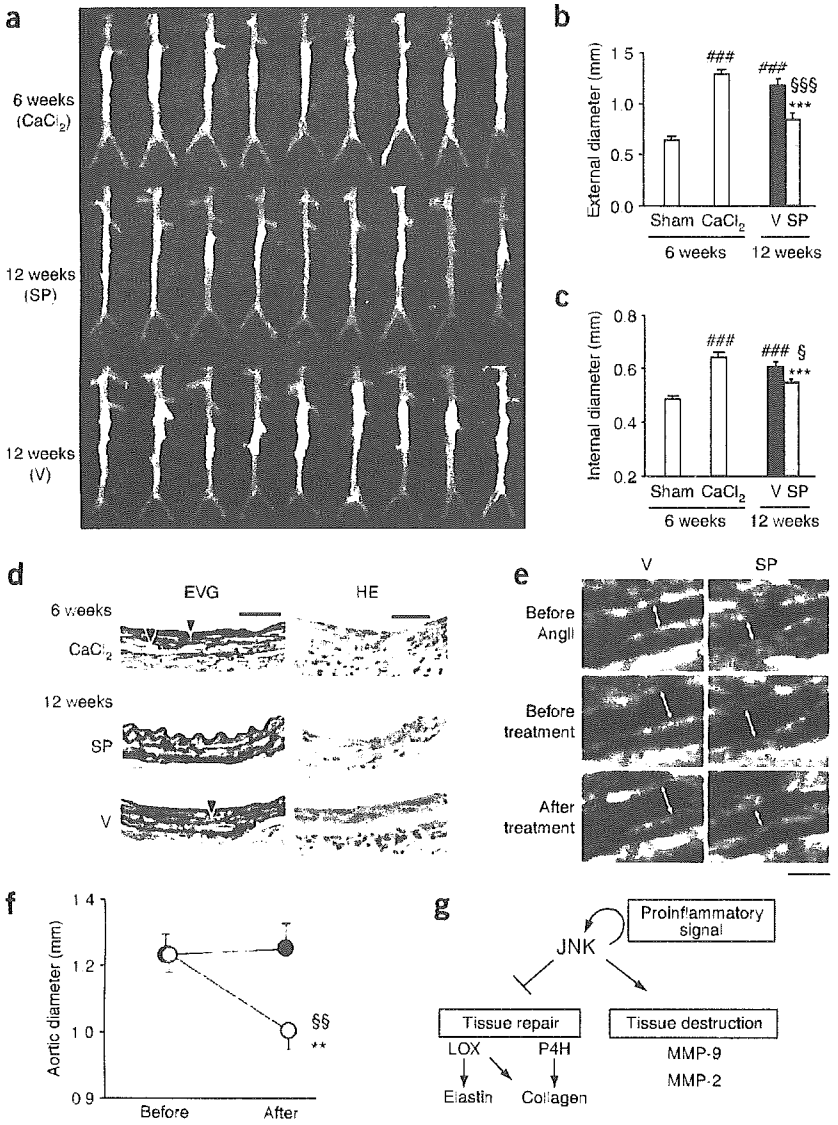

Figure 5 Regression of AAA by JNK inhibition. (**a**) AAA was established 6 weeks after the $CaCl_2$ treatment. SP600125 (SP) or vehicle (V) treatment was continued from 6 to 12 weeks after the $CaCl_2$ treatment. (**b**,**c**) External (**b**) and internal aortic diameters (**c**) were determined 6 weeks after the $CaCl_2$ treatment or sham operation (white columns), and after an additional 6 weeks of vehicle (black columns) or SP600125 (gray columns) treatment. Data are means ± s.e.m. ($n = 9$). $^{***}P < 0.001$ compared with those at 6 weeks after $CaCl_2$ treatment. $^{§}P < 0.05$ and $^{§§§}P < 0.001$, compared with vehicle treatment. $^{###}P < 0.001$, compared with sham operation. (**d**) Representative images are shown for elastica von Gieson (EVG) and H&E staining. Arrowheads indicate disrupted elastic lamellae. Scale bars, 40 μm. (**e**) Representative images of serial ultrasonographic studies are shown for the same regions in *Apoe*$^{-/-}$ mice before and after AngII infusion (before treatment) and after vehicle (V) or SP600125 (SP) treatment. Arrows indicate the lumen of aortae. Scale bar, 2 mm. (**f**) Quantitative analysis of the internal aortic diameter is shown for AngII-induced aneurysm before and after the vehicle (black circles) or SP600125 treatment (gray circles). Data are means ± s.e.m. ($n = 8$). $^{**}P < 0.01$ compared with the aortic diameter before SP600125 treatment, $^{§§}P < 0.01$ compared with the aortic diameter after vehicle treatment. (**g**) Central role of JNK in the development and progression of AAA. Schematic shows that JNK participates in the proinflammatory signals and controls both tissue repair and destruction.

activity ameliorates development of AAA. These data show that activation of JNK suppresses the expression of enzymes involved in the biosynthesis of ECM in VSMCs. Furthermore, continuous suppression of Lox activity seems to be crucial in the pathogenesis of AAA, as a transient increase in Lox activity prevents formation of AAA *in vivo*. Thus, JNK might promote formation of AAA by attenuating biosynthesis of ECM through suppression of essential enzymes.

Regression of AAA by JNK inhibition

Our *in vivo* data indicate that the ECM biosynthetic enzyme Lox is suppressed during the development of AAA when JNK is activated, whereas our *in vitro* data suggested JNK may be responsible for the suppression of ECM biosynthesis. If this notion holds true in the *in vivo* context, JNK inhibition may cause regression of established AAA by enhancing ECM biosynthesis. We tested this hypothesis in mouse AAA. Aortic morphometry showed significant dilation of the aorta 6 weeks after $CaCl_2$ treatment ($n = 9$, **Fig. 5a–c**). We began SP600125 ($n = 9$) or vehicle treatment ($n = 9$) at 6 weeks and continued it for an additional 6 weeks. Vehicle treatment resulted in no significant changes in aortic diameters (**Fig. 5a–c**), indicating that $CaCl_2$-induced AAA was fully established at 6 weeks and was maintained for an additional 6 weeks. In contrast, treatment with SP600125 caused a marked reduction in the aneurismal size compared with vehicle treatment as well as before SP600125 treatment (**Fig. 5a–c**). Histological analyses showed disrupted and flattened elastic lamellae 6 weeks after $CaCl_2$ treatment, which persisted for an additional 6 weeks with vehicle treatment (**Fig. 5d**). In contrast, SP600125-treated aortae showed a wavy morphology with less disruption of the elastic lamellae (**Fig. 5d**), indicating that JNK inhibition enhances repair of tissue architecture. In addition, JNK inhibition reduced cellular infiltration in the periaortic tissue (**Fig. 5d**) with fewer macrophages (data not shown). These data indicate that JNK inhibition causes regression of established AAA.

We tested the effect of JNK inhibition in another model of AAA created by continuous infusion of AngII in hyperlipidemic mice[26]. This model of AAA is advantageous because AAA develops in the suprarenal aorta, allowing accurate and repeated assessment by non-invasive ultrasonography (**Supplementary Fig. 5** online). We started AngII infusion at 6 months of age in male apolipoprotein E–null (*Apoe*$^{-/-}$) mice and continued it for 4 weeks. We assigned these mice to two groups with equivalent aortic diameters after AngII infusion (1.23 ± 0.06 mm, $n = 8$ (vehicle group) versus 1.23 ± 0.05 mm, $n = 8$ (SP group)), and treated the mice with vehicle or SP600125 for an additional 8 weeks. Notably, seven out of eight mice in the SP group

showed a reduction in aortic diameter, resulting in an 18.0% reduction of aortic diameter ($P < 0.01$, paired t-test) during the 8 weeks of treatment (**Fig. 5e,f**). In contrast, the vehicle-treated group showed no significant change in aortic diameter (+1.5%, **Fig. 5e,f**), indicating that AAA was established during 4 weeks of AngII infusion. SP600125 did not cause a significant change in atheroma area (data not shown) nor in systolic blood pressure (**Supplementary Fig. 5** online). These data indicate that JNK inhibition causes regression of AngII-induced AAA after its establishment.

DISCUSSION

Our data indicate that JNK is a proximal signaling molecule in the pathogenesis of AAA, a chronic inflammatory disease characterized by disruption of the ECM. Recent studies showed that macrophage-derived MMP-9 and interstitial cell–derived MMP-2 work in concert toward the development of experimental AAA in mice[4]. We showed that JNK activity is crucial for secretion of these MMPs in both cell types. In addition, the JNK pathway may participate in the proinflammatory cascade[24] in AAA. Consequently, inhibition of JNK resulted in the marked suppression of MMP activities, cellular infiltration and AAA development in mice. The role of JNK in MMP-9 expression is consistent with studies in tumor cell lines[27–29]. Our results, however, indicate a much wider role for JNK in ECM metabolism than previously thought, providing an explanation for effective regression of AAA by JNK inhibition.

One unexpected finding in this study was that JNK suppressed genes encoding crucial ECM biosynthetic enzymes, including *Lox* and *P4ha1*. It has been hypothesized that impaired ECM biosynthesis in addition to degradation of the ECM may have an important role in pathogenesis of AAA[7]. Reduced Lox expression in experimental AAA has been shown in a previous study[7] and here, which may explain ineffective maturation of the ECM in human AAA[6,9]. One of the potential mechanisms for JNK-mediated suppression of ECM biosynthesis is antagonism of JNK against transforming growth factor (TGF)-β[30,31] that activates ECM biosynthesis in VSMCs[32] and stabilizes experimental AAA[33]. In fact, *Jnk2*$^{-/-}$ VSMCs secrete higher amounts of TGF-β than wild-type VSMCs (K.Y. & H.A., unpublished observation). Another potential mechanism is JNK-mediated apoptosis of VSMCs, as proposed for cerebral aneurysms[34]. Suppression of ECM biosynthesis by JNK, however, is probably independent of JNK-mediated apoptosis, as JNK-activated VSMCs did not show a higher rate of cell death under the conditions of our experiments.

Inhibition of MMPs[7,10–14] and NF-κB[35,36] has been reported to prevent the development of experimental AAA. JNK may be involved in the molecular events after these interventions. For example, doxycycline, an inhibitor of MMPs, inhibits JNK activity and MMP-9 expression in corneal epithelial cells[37]. This may be the molecular mechanism for the preventive effect of doxycycline in AAA[7,11], in addition to its direct inhibition of MMPs. NF-κB synergistically regulates the expression of MMP-9 with AP-1 (ref. 38), which is the major target of JNK pathway. NF-κB and the JNK pathway, however, may not always work synergistically, because NF-κB antagonizes the JNK pathway in TNF-α–induced apoptosis (reviewed in ref. 39), showing the complicated signaling network between these pathways. Elucidation of the details of JNK-related molecular events may identify further potential therapeutic targets for AAA and other diseases with destructive ECM metabolism.

These data taken together show that inhibition of JNK ameliorates catastrophic ECM metabolism and enhances tissue repair (**Fig. 5g**), resulting in effective regression of AAA *in vivo*. JNK-targeted therapy may provide nonsurgical therapeutic options for AAA, a disease that frequently results in a fatal outcome.

METHODS

Mouse model of AAA. We induced AAA in mice by periaortic application of 0.5 M $CaCl_2$ as described previously[7]. For the prevention study, we treated mice with subcutaneous injection of SP600125 (30 mg/kg) in PPCES buffer (**Supplementary Methods** online; $n = 8$)[40] or vehicle ($n = 8$) twice daily for 10 weeks. The sham group received saline instead of $CaCl_2$ ($n = 8$). For the regression study, we treated 27 mice with $CaCl_2$. We performed aortic morphometry for nine mice 6 weeks after $CaCl_2$ treatment. We began an additional 6 weeks of SP600125 ($n = 9$) or vehicle ($n = 9$) treatment 6 weeks after $CaCl_2$ treatment. We created AngII-induced AAA by continuous infusion of AngII (1,000 ng/min/kg) for 4 weeks in *Apoe*$^{-/-}$ mice, as reported previously[26]. At the end of AngII infusion, we determined aortic diameter by ultrasonography to divide the mice into two groups with equivalent average AAA diameters. One group received SP600125 ($n = 8$) and the other group received vehicle ($n = 8$) for an additional 8 weeks. We monitored systolic blood pressure by the tail cuff method (BP-98A, Softron). We determined the diameter of AngII-induced AAA in live mice using the HDI 5000 system (Philips) equipped with a 15 MHz linear probe by an operator who was blinded to the experimental conditions. We identified the aorta by color Doppler imaging and located the aneurysm using anatomical landmarks. After the observation period, mice were killed by an overdose of pentobarbital and were perfusion-fixed with a mixture of 3.7% formaldehyde in PBS at physiological perfusion pressure. We determined the internal diameter of aortae by X-ray aortograms with Softex-C60 (Softex). We excised abdominal aortae, photographed them to determine the external diameter and used them for histological analyses. All aortic morphometry was performed by an investigator blinded to the experimental groups. We performed adenoviral gene transfer by treating aorta with 20 μl of Ad-Lox ($n = 8$) or Ad-*lacZ* ($n = 5$) at the same titer (1.5×10^9 plaque-forming units/ml) 3 weeks after $CaCl_2$ treatment, followed by aortic morphometry after an additional 3 weeks. Animal experimental protocols were approved by Yamaguchi University School of Medicine Animal Review Board.

Human aortic samples. We obtained surgical specimens from individuals with AAA or AOD or autopsy specimens from individuals who died of unrelated causes. For *ex vivo* culture, we obtained fresh AAA samples during surgery and minced them to approximately 1 mm thick. We maintained equal wet weight of the minced tissue in each well of the 6-well plates with DMEM (Invitrogen). We collected the conditioned media from 48 to 96 h after treatment with or without 100 ng/ml TNF-α (R&D Systems) and 50 μM SP600125. All protocols using human specimens were approved by the Institutional Review Board at Yamaguchi University Hospital and the samples were obtained with informed consent.

Cell culture. We prepared and maintained rat or mouse aortic VSMCs in DMEM with 10% FBS[23,31]. We maintained THP-1 cells in RPMI1640 containing 10% FBS. We used Ad-dnJnk1 (multiplicity of infection (MOI) 30), 50 μM SP600125 (Tocris) or 20 μM D-stereoisomer of JNK inhibitor-1 (D-JNK-I-1, Alexis)[25] to inhibit JNK activities.

Adenoviral vectors. We constructed adenoviral vectors encoding green fluorescent protein (Ad-GFP), β-galactosidase (Ad-*lacZ*), constitutively active MKK7 (Ad-caMkk7), wild-type JNK1 (Ad-Jnk1), dominant negative JNK1 (Ad-dnJnk1) and Lox (Ad-Lox) as previously described[12]. Ad-GFP or Ad-*lacZ* served as a negative control.

Transcriptional analyses. We isolated total RNA using RNeasy (Qiagen). We performed two sets of DNA microarray analyses using GeneChip Rat Genome U34A (Affymetrix) and Affymetrix Microarray Analysis Suite (MAS) 4.0 at BIDMC Genomics Center as follows.

For the caMKK7 set, we infected VSMCs with Ad-caMkk7 (MOI 15) and Ad-Jnk1 (MOI 15) to specifically activate the JNK pathway, or we infected them with Ad-GFP (MOI 30) as a control.

For the dnJNK set, we infected VSMCs with Ad-dnJnk1 (MOI 30) to specifically inhibit the JNK pathway, or we infected them with Ad-GFP (MOI 30) as a control, followed by stimulation with 100 μM H_2O_2.

We normalized the signal intensities using the average signal intensity of each array so that direct comparison could be made between arrays. We obtained *P* values for the caMKK7 set (P_{caMKK7}) and the dnJNK set (P_{dnJNK}) using Affymetrix MAS1.0, which indicate the statistical significance of the changes in the gene expression in each set. We defined JNK-dependence index using the following equation (**Supplementary Fig. 1** online): JNK Dependence Index = (R_{caMKK7}/R_{dnJNK} or R_{dnJNK}/R_{caMKK7}, whichever is less) $\times \sqrt{(R^2_{caMKK7} + R^2_{dnJNK})}$. We performed gene-specific mRNA analyses by northern analyses or quantitative RT-PCR (for primers, see **Supplementary Methods** online) using a Light Cycler (Roche). *Gapdh* mRNA served as an internal control in each reaction. Normalization with cyclophilin A mRNA (*Ppia*) resulted in identical results.

Protein analyses. We rinsed human or mouse aortic specimens in PBS, homogenized them in a homogenizing buffer (**Supplementary Methods** online) and then added Triton X-100 to the final concentration of 1% to extract proteins. We determined protein concentrations in the samples by BCA protein assay kit (Pierce) and we loaded an equal amount of protein on each lane of SDS-PAGE. We performed western blotting and immunostaining using commercially available antibodies (**Supplementary Methods** online). GAPDH signal served as an internal control for protein loading in western blotting. We performed gelatin zymography of the conditioned media as previously described[13] to analyze MMP-2 and MMP-9 (**Supplementary Methods** online). We determined activity of native MMP-9 in the conditioned media by first immunocapturing MMP-9 on the assay plate and then applying chromogenic substrate using MMP-9 Activity Assay System (Amersham Biosciences), and detected the degradation product of collagen IV by ELISA (Daiichi Fine Chemical). For the Lox activity assay, we homogenized mouse aortic specimens in PBS and extracted them in a buffer containing 6 M urea and 50 mM sodium borate (pH 8.2). We measured the Lox activity as described previously[14], normalized for the tissue wet weight and expressed it as fold changes compared with the first time point of the experiments.

Statistics. All data are expressed as means ± s.e.m. Statistical analysis was performed using analysis of variance (ANOVA) unless otherwise stated. The post-test comparison was performed by the method of Fisher.

Accession codes. Gene Expression Omnibus, GSE2190.

Note: Supplementary information is available on the Nature Medicine website.

ACKNOWLEDGMENTS

We thank D. Boyle and G.S. Firestein for suggestions, S. Saito, M. Oishi and T. Hozawa for technical assistance and E.O. Weinberg, H. Suzuki and H. Oda for critical reading. This work was supported in part by Grant-in-aid for Scientific Research (KAKENHI 12770651, 14657284 and 17591337 (to K.Y.), 12670673, 12204081, 14370229 and 16390365 (to H.A.), 12770344 (to K.E.) and 16209026 (to M.M.)) from MEXT Japan, Japan Heart Foundation/Zeria Pharmaceutical Grant for Research on Cardiovascular Disease (to H.A.), New Frontier Project from Yamaguchi University (to H.A. and K.Y.) and a Grant from Sankyo Company for the Department of Molecular Cardiovascular Biology, Yamaguchi University School of Medicine.

COMPETING INTERESTS STATEMENT

The authors declare that they have no competing financial interests.

Published online at http://www.nature.com/naturemedicine/
Reprints and permissions information is available online at http://npg.nature.com/reprintsandpermissions/

1. Curci, J.A., Lee, J.K. & Thompson, R.W. Pathogenesis of Abdominal Aortic Aneurysm. in *Current Therapy in Vascular Surgery* (eds. Ernst, C.B. & Stanley, J.C.) 199–206 (Elsevier, Philadelphia, 2001).
2. Upchurch, G.R., Jr. Gene therapy to treat aortic aneurysms: right goal, wrong strategy. *Circulation* **112**, 939–940 (2005).
3. Pyo, R. *et al.* Targeted gene disruption of matrix metalloproteinase-9 (gelatinase B) suppresses development of experimental abdominal aortic aneurysms. *J. Clin. Invest.* **105**, 1641–1649 (2000).
4. Longo, G.M. *et al.* Matrix metalloproteinases 2 and 9 work in concert to produce aortic aneurysms. *J. Clin. Invest.* **110**, 625–632 (2002).
5. Allaire, E., Forough, R., Clowes, M., Starcher, B. & Clowes, A.W. Local overexpression of TIMP-1 prevents aortic aneurysm degeneration and rupture in a rat model. *J. Clin. Invest.* **102**, 1413–1420 (1998).
6. Krettek, A., Sukhova, G.K. & Libby, P. Elastogenesis in human arterial disease: a role for macrophages in disordered elastin synthesis. *Arterioscler. Thromb. Vasc. Biol.* **23**, 582–587 (2003).
7. Huffman, M.D. *et al.* Functional importance of connective tissue repair during the development of experimental abdominal aortic aneurysms. *Surgery* **128**, 429–438 (2000).
8. Rowe, D., McGoodwin, E., Martin, G. & Grahn, D. Decreased lysyl oxidase activity in the aneurysm-prone, mottled mouse. *J. Biol. Chem.* **252**, 939–942 (1977).
9. Bode, M.K. *et al.* Increased amount of type III pN-collagen in AAA when compared with AOD. *Eur. J. Vasc. Endovasc. Surg.* **23**, 413–420 (2002).
10. Bigatel, D.A. *et al.* The matrix metalloproteinase inhibitor BB-94 limits expansion of experimental abdominal aortic aneurysms. *J. Vasc. Surg.* **29**, 130–138 (1999).
11. Petrinec, D. *et al.* Doxycycline inhibition of aneurysmal degeneration in an elastase-induced rat model of abdominal aortic aneurysm: preservation of aortic elastin associated with suppressed production of 92 kD gelatinase. *J. Vasc. Surg.* **23**, 336–346 (1996).
12. Prall, A.K. *et al.* Doxycycline in patients with abdominal aortic aneurysms and in mice: comparison of serum levels and effect on aneurysm growth in mice. *J. Vasc. Surg.* **35**, 923–929 (2002).
13. Mosorin, M. *et al.* Use of doxycycline to decrease the growth rate of abdominal aortic aneurysms: a randomized, double-blind, placebo-controlled pilot study. *J. Vasc. Surg.* **34**, 606–610 (2001).
14. Baxter, B.T. *et al.* Prolonged administration of doxycycline in patients with small asymptomatic abdominal aortic aneurysms: report of a prospective (Phase II) multicenter study. *J. Vasc. Surg.* **36**, 1–12 (2002).
15. Allaire, E. *et al.* Vascular smooth muscle cell endovascular therapy stabilizes already developed aneurysms in a model of aortic injury elicited by inflammation and proteolysis. *Ann. Surg.* **239**, 417–427 (2004).
16. Buth, J. & Harris, P. Endovascular Treatment of Aortic Aneurysms. in *Vascular Surgery* (ed. Rutherford, R.B.) 1452–1475 (Elsevier, Philadelphia, 2005).
17. Patel, M.I., Melrose, J., Ghosh, P. & Appleberg, M. Increased synthesis of matrix metalloproteinases by aortic smooth muscle cells is implicated in the etiopathogenesis of abdominal aortic aneurysms. *J. Vasc. Surg.* **24**, 82–92 (1996).
18. Manning, A.M. & Davis, R.J. Targeting JNK for therapeutic benefit: from junk to gold? *Nat. Rev. Drug Discov.* **2**, 554–565 (2003).
19. Galis, Z.S. & Khatri, J.J. Matrix metalloproteinases in vascular remodeling and atherogenesis: the good, the bad, and the ugly. *Circ. Res.* **90**, 251–262 (2002).
20. Mietus-Snyder, M., Glass, C.K. & Pitas, R.E. Transcriptional activation of scavenger receptor expression in human smooth muscle cells requires AP-1/c-Jun and C/EBPbeta. *Arterioscler. Thromb. Vasc. Biol.* **18**, 1440–1449 (1998).
21. Yan, L., Borregaard, N., Kjeldsen, L. & Moses, M.A. The high molecular weight urinary matrix metalloproteinase (MMP) activity is a complex of gelatinase B/MMP-9 and neutrophil gelatinase-associated lipocalin (NGAL). Modulation of MMP-9 activity by NGAL. *J. Biol. Chem.* **276**, 37258–37265 (2001).
22. Maki, J. *et al.* Inactivation of the lysyl oxidase gene Lox leads to aortic aneurysms, cardiovascular dysfunction, and perinatal death in mice. *Circulation* **106**, 2503–2509 (2002).
23. Ricci, R. *et al.* Requirement of JNK2 for scavenger receptor A-mediated foam cell formation in atherogenesis. *Science* **306**, 1558–1561 (2004).
24. Bagowski, C.P. & Ferrell, J.E., Jr. Bistability in the JNK cascade. *Curr. Biol.* **11**, 1176–1182 (2001).
25. Borsello, T. *et al.* A peptide inhibitor of c-Jun N-terminal kinase protects against excitotoxicity and cerebral ischemia. *Nat. Med.* **9**, 1180–1186 (2003).
26. Daugherty, A., Manning, M.W. & Cassis, L.A. Angiotensin II promotes atherosclerotic lesions and aneurysms in apolipoprotein E-deficient mice. *J. Clin. Invest.* **105**, 1605–1612 (2000).
27. Shin, M. *et al.* An inhibitor of c-jun aminoterminal kinase (SP600125) represses c-Jun activation, DNA-binding and PMA-inducible 92-kDa type IV collagenase expression. *Biochim. Biophys. Acta* **1589**, 311–316 (2002).
28. Gum, R., Wang, H., Lengyel, E., Juarez, J. & Boyd, D. Regulation of 92 kDa type IV collagenase expression by the jun aminoterminal kinase- and the extracellular signal-regulated kinase-dependent signaling cascades. *Oncogene* **14**, 1481–1493 (1997).
29. Cho, A., Graves, J. & Reidy, M.A. Mitogen-activated protein kinases mediate matrix metalloproteinase-9 expression in vascular smooth muscle cells. *Arterioscler. Thromb. Vasc. Biol.* **20**, 2527–2532 (2000).
30. Ventura, J.J., Kennedy, N.J., Flavell, R.A. & Davis, R.J. JNK regulates autocrine expression of TGF-beta1. *Mol. Cell* **15**, 269–278 (2004).
31. Leask, A., Holmes, A., Black, C.M. & Abraham, D.J. Connective tissue growth factor gene regulation. Requirements for its induction by transforming growth factor-beta 2 in fibroblasts. *J. Biol. Chem.* **278**, 13008–13015 (2003).
32. Schlumberger, W., Thie, M., Rauterberg, J. & Robenek, H. Collagen synthesis in cultured aortic smooth muscle cells. Modulation by collagen lattice culture, transforming growth factor-beta 1, and epidermal growth factor. *Arterioscler. Thromb.* **11**, 1660–1666 (1991).
33. Dai, J. *et al.* Overexpression of transforming growth factor-beta1 stabilizes already-formed aortic aneurysms: a first approach to induction of functional healing by endovascular gene therapy. *Circulation* **112**, 1008–1015 (2005).
34. Takagi, Y., Ishikawa, M., Nozaki, K., Yoshimura, S. & Hashimoto, N. Increased expression of phosphorylated c-Jun amino-terminal kinase and phosphorylated c-Jun in human cerebral aneurysms. *Neurosurgery* **51**, 997–1002 (2002).

35. Parodi, F.E., Mao, D., Ennis, T.L., Bartoli, M.A. & Thompson, R.W. Suppression of experimental abdominal aortic aneurysms in mice by treatment with pyrrolidine dithiocarbamate, an antioxidant inhibitor of nuclear factor-kappaB. *J. Vasc. Surg.* **41**, 479–489 (2005).
36. Nakashima, H. *et al.* Inhibition of experimental abdominal aortic aneurysm in the rat by use of decoy oligodeoxynucleotides suppressing activity of nuclear factor kappaB and ets transcription factors. *Circulation* **109**, 132–138 (2004).
37. Kim, H.S., Luo, L., Pflugfelder, S.C. & Li, D.Q. Doxycycline inhibits TGF-beta1-induced MMP-9 via Smad and MAPK pathways in human corneal epithelial cells. *Invest. Ophthalmol. Vis. Sci.* **46**, 840–848 (2005).
38. Sato, H. & Seiki, M. Regulatory mechanism of 92 kDa type IV collagenase gene expression which is associated with invasiveness of tumor cells. *Oncogene* **8**, 395–405 (1993).
39. Papa, S., Zazzeroni, F., Pham, C.G., Bubici, C. & Franzoso, G. Linking JNK signaling to NF-kappaB: a key to survival. *J. Cell Sci.* **117**, 5197–5208 (2004).
40. Bennett, B.L. *et al.* SP600125, an anthrapyrazolone inhibitor of Jun N-terminal kinase. *Proc. Natl. Acad. Sci. USA* **98**, 13681–13686 (2001).
41. Adachi, M. *et al.* Proteasome-dependent decrease in Akt by growth factors in vascular smooth muscle cells. *FEBS Lett.* **554**, 77–80 (2003).
42. Aoki, H. *et al.* Direct activation of mitochondrial apoptosis machinery by c-Jun N-terminal kinase in adult cardiac myocytes. *J. Biol. Chem.* **277**, 10244–10250 (2002).
43. Zempo, N. *et al.* Matrix metalloproteinases of vascular wall cells are increased in balloon-injured rat carotid artery. *J. Vasc. Surg.* **20**, 209–217 (1994).
44. Palamakumbura, A.H. & Trackman, P.C. A fluorometric assay for detection of lysyl oxidase enzyme activity in biological samples. *Anal. Biochem.* **300**, 245–251 (2002).

Circulation
JOURNAL OF THE AMERICAN HEART ASSOCIATION

American Heart Association
Learn and Live

Correction of Defective Interdomain Interaction Within Ryanodine Receptor by Antioxidant Is a New Therapeutic Strategy Against Heart Failure

Masafumi Yano, Shinichi Okuda, Tetsuro Oda, Takahiro Tokuhisa, Hiroki Tateishi, Mamoru Mochizuki, Toshiyuki Noma, Masahiro Doi, Shigeki Kobayashi, Takeshi Yamamoto, Yasuhiro Ikeda, Tomoko Ohkusa, Noriaki Ikemoto and Masunori Matsuzaki

Circulation 2005;112;3633-3643
DOI: 10.1161/CIRCULATIONAHA.105.555623
Circulation is published by the American Heart Association. 7272 Greenville Avenue, Dallas, TX 72514
 Print ISSN: 0009-7322. Online ISSN: 1524-4539

Correction of Defective Interdomain Interaction Within Ryanodine Receptor by Antioxidant Is a New Therapeutic Strategy Against Heart Failure

Masafumi Yano, MD, PhD; Shinichi Okuda, MD, PhD; Tetsuro Oda, MD; Takahiro Tokuhisa, MD; Hiroki Tateishi, MD; Mamoru Mochizuki, MD; Toshiyuki Noma, BS; Masahiro Doi, MD, PhD; Shigeki Kobayashi, MD, PhD; Takeshi Yamamoto, MD, PhD; Yasuhiro Ikeda, MD, PhD; Tomoko Ohkusa, MD, PhD; Noriaki Ikemoto, PhD; Masunori Matsuzaki, MD, PhD

Background—Defective interdomain interaction within the ryanodine receptor (RyR2) seems to play a key role in the pathogenesis of heart failure, as shown in recent studies. In the present study we investigated the effect of oxidative stress on the interdomain interaction, its outcome in the cardiac function in heart failure, and the possibility of preventing the problem with antioxidants.

Methods and Results—Sarcoplasmic reticulum (SR) vesicles were isolated from dog left ventricular (LV) muscle (normal or rapid ventricular pacing for 4 weeks with or without the antioxidant edaravone). In the edaravone-treated paced dogs (EV+), but not in the untreated paced dogs (EV−), normal cardiac function was restored almost completely. In the SR vesicles isolated from the EV−, oxidative stress of the RyR2 (reduction in the number of free thiols) was severe, but it was negligible in EV+. The oxidative stress of the RyR2 destabilized interdomain interactions within the RyR2 (EV−), but its effect was reversed in EV+. Abnormal Ca^{2+} leak through the RyR2 was found in EV− but not in EV+. The amount of the RyR2-bound FKBP12.6 was less in EV− than in normal dogs, whereas it was restored almost to a normal amount in EV+. The NO donor 3-morpholinosydnonimine (SIN-1) reproduced, in normal SR, several abnormal features seen in failing SR, such as defective interdomain interaction and abnormal Ca^{2+} leak. Both cell shortening and Ca^{2+} transients were impaired by SIN-1 in isolated normal myocytes, mimicking the pathophysiological conditions in failing myocytes. Incubation of failing myocytes with edaravone restored the normal properties.

Conclusions—During the development of heart failure, edaravone ameliorated the defective interdomain interaction of the RyR2. This prevented Ca^{2+} leak and LV remodeling, leading to an improvement of cardiac function and an attenuation of LV remodeling. **(*Circulation*. 2005;112:3633-3643.)**

Key Words: calcium ■ free radicals ■ heart failure ■ sarcoplasmic reticulum

A considerable body of evidence suggests that an abnormal regulation of the intracellular Ca^{2+} by the sarcoplasmic reticulum (SR) is the chief pathogenic mechanism for various types of dysfunctions seen in heart failure. In our recent studies of the canine model of pacing-induced heart failure, we have demonstrated that the Ca^{2+}-release function of the ryanodine receptor (RyR2) is defective in heart failure, presumably because of a partial loss of FKBP12.6 from the RyR2, and this defective regulation of the RyR2 causes an abnormal Ca^{2+} leak by mediation of a conformational change in the RyR2.[1] Marx et al[2] demonstrated that protein kinase A (PKA)–mediated hyperphosphorylation of the RyR2 causes dissociation of FKBP12.6 from the RyR2, resulting in a defective channel function due to an increased sensitivity to Ca^{2+}-induced activation. In failing hearts, reduced levels of PP1 and PP2A in the RyR2 macromolecular complex rather than increased PKA activity appear to be responsible for the RyR2 hyperphosphorylation and the formation of "leaky" channels.[2] We found that both β-blockers[3] and a new cardioprotective agent, JTV519,[4,5] correct the defective FKBP12.6-mediated control of the RyR2, improving cardiac function during the development of heart failure. Wehrens et al[6] also demonstrated that JTV519 increased the binding affinity of FKBP12.6 to the RyR2, which stabilized the closed state of the RyR2 channels and prevented the abnormal Ca^{2+} leak that would otherwise have triggered ventricular arrhythmias. These studies suggest that securing the FKBP12.6-mediated stabilization of the RyR2 may be a new therapeutic strategy against heart failure.

Received April 13, 2005; revision received September 13, 2005; accepted September 19, 2005.

From the Department of Medical Bioregulation, Division of Cardiovascular Medicine, Yamaguchi University School of Medicine, Yamaguchi, Japan (M.Y., S.O., T. Oda, T.T., H.T., M. Mochizuki, T.N., M.D., S.K., T.Y., Y.I., T. Ohkusa, M. Matsuzaki); Boston Biomedical Research Institute, Watertown, Mass (N.I.); and Department of Neurology, Harvard Medical School, Boston, Mass (N.I.).

Correspondence to Masafumi Yano, MD, PhD, Department of Medical Bioregulation, Division of Cardiovascular Medicine, Yamaguchi University School of Medicine, 1-1-1 Minamikogushi, Ube, Yamaguchi 755-8505, Japan. E-mail yanoma@yamaguchi-u.ac.jp

Circulation **is available at http://www.circulationaha.org** **DOI: 10.1161/CIRCULATIONAHA.105.555623**

Recently, it has been demonstrated that the mode of interdomain interaction of 2 specific domains within the RyR2 (N-terminal and central domains), which contain several mutations reported in arrhythmogenic right ventricular cardiomyopathy type 2 (ARVD/C2) and polymorphic ventricular tachycardia,[7-9] plays a key role in Ca^{2+} channel regulation and in the pathogenesis of heart failure. In normal operation, the interaction of these domains is tight (zipped), stabilizing the closed state of the channel; on stimulation of the RyR2, the interdomain interaction becomes loose (unzipped), and the channel opens.[10] In diseased conditions, a mutation in either of these domains weakens the interdomain interaction even in resting or nonactivating conditions, and diseased channels remain partially open. As shown in our recent study of the pacing-induced heart failure model,[11] abnormal interdomain interaction as well as dissociation of the RyR2-bound FKBP12.6 destabilizes the channel gating of the RyR2 and then produces Ca^{2+} leak, suggesting that the weakened interdomain interaction is one of the key mechanisms underlying the pathogenesis of ARVD/C2, polymorphic ventricular tachycardia, and heart failure.

It has been suggested that oxygen free radicals, produced by the reduction of oxygen during many cellular reactions, are involved in the pathogenesis of a variety of cardiovascular diseases, including heart failure.[12] Highly reactive free radicals have a severe effect on many cellular structures and on a variety of important cellular functions. Recently, it has been suggested that RyR channel gating is regulated by the redox state and that oxidation or nitrosylation of the cysteine residues in the RyR produces considerable changes in channel function.[13]

Edaravone (3-methyl-1-phenyl-2-pyrazolin-5-one; MCI-186), a synthetic antioxidant, is a ubiquitously acting direct free radical scavenger. Because of its highly efficient function of detoxifying the devastatingly reactive ·OH, edaravone directly neutralizes peroxyl radicals (LOO·).[14] We hypothesized that in heart failure the production of oxygen free radicals may affect the channel regulation of the RyR2 and cause abnormal contractile and relaxation function. If this is the case, edaravone, because of its antioxidant effect, may restore normal channel gating in the failing RyR2, thereby preventing the development of heart failure.

In the present study we tested this hypothesis by investigating the effects of oxidative stress on several key factors that are likely involved in the pathogenesis, such as the interdomain interaction and the RyR2-associated FKBP12.6, as described above. As shown here, the NO donor 3-morpholinosydnonimine (SIN-1) produced, in the normal SR, the same type of dysfunctions as seen in the SR from the failing heart (pacing-induced heart failure), such as destabilization of interdomain interaction, partial dissociation of FKBP12.6, and Ca^{2+} leak. Interestingly, the antioxidant edaravone reversed all 3 of these problems in pacing-induced heart failure.

Methods

Materials

FK506, edaravone, SEA0400, and JTV519 were provided by Fujisawa Pharmaceutical Co Ltd, Mitsubishi Pharma Corporation Co Ltd, Taisho Pharmaceutical Co, Ltd, and Aetas Pharmaceutical Co Ltd, respectively.

Animal Preparation

In beagle dogs weighing 10 to 13 kg, heart failure was induced by 28 days of rapid ventricular (RV) pacing at 250 bpm (referred to as 4W pacing) with the use of an externally programmable miniature pacemaker (Medtronic Inc), and both left ventricular (LV) pressure and 2-dimensional echocardiograms were measured in the conscious state, as described elsewhere.[1,3,4] The long-term administration of the antioxidant edaravone (0.6 mg/kg per day IV) was immediately followed by the initiation of RV pacing. The care of the animals and the protocols used were in accordance with guidelines of the Animal Ethics Committee of Yamaguchi University School of Medicine.

Preparation of SR Vesicles

SR vesicles were prepared from dog LV, as described elsewhere.[1,3,4]

Ca^{2+} Uptake and Leak Assays

Ca^{2+} uptake and Ca^{2+} leak assays were performed as described previously.[1,3,4]

[^{3}H]Dihydro-FK506 and [^{3}H]Ryanodine Binding Assays

[^{3}H]Dihydro-FK506 and [^{3}H]ryanodine (Dupont NEN) binding assays were performed as described elsewhere.[1,3,4]

Peptides Used and Peptide Synthesis

We used a synthetic peptide corresponding to residues 2460 to 2495 of the RyR2, DPc10, that includes 1 residue mutable in polymorphic ventricular tachycardia, as described previously[11,15]: 2459GPCP-DHKAAMVLFLD*R*VYGIEVQDFLLHLLEVGFLP2494.

The peptide was synthesized on an Applied Biosystems model 431A synthesizer with the use of Fmoc [*N*-(9-fluorenyl)methoxycarbonyl] as the α-amino protecting group, as described previously.[15]

Site-Directed Fluorescence Labeling of the RyR2

Specific fluorescence labeling of the RyR2 moiety of the SR was performed with the use of the cleavable hetero-bifunctional cross-linking reagent sulfosuccinimidyl 3-([2-(7-azido-4-methylcoumarin-3-acetamido)ethyl]dithio)propionate (SAED) from PIERCE, with DPc10 as a site-specific carrier, as described previously.[11,16]

Fluorescence Quenching of the Methylcoumarin Acetate Probe Attached to the DPc10 Binding Site

The zipped and unzipped states of the interacting domains of the RyR2 were assessed by the fluorescence quench technique described previously.[11,16] The principle of the fluorescence quench assay of domain unzipping is that a large-size quencher BSA-QSY is inaccessible to the attached methylcoumarin acetate in the zipped state, whereas it becomes accessible to the methylcoumarin acetate site in the unzipped state. To form the quencher, QSY 7 carboxylic acid was conjugated with BSA by incubating 5 mmol/L QSY 7 carboxylic acid with 0.5 mmol/L BSA in 20 mmol/L HEPES (pH 7.5) for 60 minutes at 22°C in the dark. Unreacted QSY 7 carboxylic acid was removed by means of Sephadex G50 gel filtration. Fluorescence quenching by both QSY 7 BSA conjugate (a large-size quencher) and acrylamide (a small-size quencher) was performed by measuring steady state fluorescence of labeled methylcoumarin acetate (excitation at 368 nm, emission at 455 nm) in the presence or absence of the quencher. The data were analyzed with the use of the Stern-Volmer equation.

Immunoblot Analysis

Immunoblot analyses for FKBP12.6, SR Ca^{2+}-ATPase, and phospholamban (PLB) were performed as described elsewhere.[1,3,4] By employing the method of Marx et al,[2] we achieved coimmunoprecipitation of FKBP12.6 from SR using anti-RyR2 antibody (Oncogene Research Products) followed by immunoblotting with anti-

TABLE 1. Hemodynamic Data

	HR, bpm	LVPSP, mm Hg	LVEDP, mm Hg	+dP/dt, mm Hg/s	Tau, ms	LVEDD, mm	LVESD, mm	LVFS, %
Edaravone-untreated (n=7)								
Prepacing	122±9	124±16	8.5±2.5	3008±190	18.2±3.8	30.8±1.2	19.2±1.1	38.0±2.1
4w pacing	118±15	116±22	35.2±2.8*	1358±214*	39.9±8.6*	40.9±2.0*	36.8±2.8*	12.2±3.3*
Edaravone-treated (n=5)								
Prepacing	132±16	124±15	7.4±2.1	3256±262	17.6±4.3	30.4±1.4	19.3±1.6	38.2±3.3
4w pacing	130±10	112±16	20.2±6.0*†	1825±215*†	26.2±3.5*‡	35.4±1.5*‡	27.1±1.5*‡	20.2±2.5*‡

HR indicates heart rate; LVPSP, LV peak-systolic pressure; LVEDP, LV end-diastolic pressure; +dP/dt, peak +dP/dt of LV pressure; Tau, time constant of LV pressure decay during isovolumic relaxation period; LVEDD, LVend-diastolic diameter; LVESD, LV end-systolic diameter, and FS, fractional shortening: (LVEDD−LVESD)/LVEDD×100. Data are mean±SD.

*$P<0.01$ vs prepacing group; †$P<0.05$, ‡$P<0.01$ vs edaravone-untreated group.

FKBP12 (C-19) antibody (Santa Cruz Biotechnology). The relative phosphorylation level of RyR was determined by immunoblotting with anti-phosphoRyR2 (P2809), which was kindly provided by Dr Andrew R. Marks (Columbia University). Specific antibodies against phosphoserine 16-phospholamban (PLB; Upstate Biotech) and an epitope common to all PLB forms (PLB; Upstate Biotech) were also used.

Oxidative Stress Level in LV Muscle and RyR2

To determine the oxidative stress level in the hearts, immunohistochemical analysis was performed with the use of mouse monoclonal anti–4-hydroxy-2-nonenal (HNE)–modified protein antibody (1:50 dilution, NOF Medical Department), according to the method of Nakamura et al.[17]

The content of free thiols (the number of reduced cysteines) in the canine RyR2 was determined with the use of the monobromobimane (mBB, Calbiochem) fluorescence technique.[18,19] SR vesicles were incubated with an excess concentration (250 μmol/L) of lipophilic, thiol-specific agent mBB for 1 hour in the dark at 24 C. The fluorescence emission intensity of the RyR2-bound mBB (ie, the thiol content) was then measured at 482 nm by exciting at 382 nm (Perkin-Elmer luminescence spectrophotometer LS50B). As a reference, matched experiments were performed in the presence of 100 μmol/L dithiothreitol (DTT).[19] The mBB fluorescence in the RyR2, expressed as a percentage of the reference, was defined as the relative content of free thiols in the RyR2.

In canine cardiac myocytes, a fluorescent probe, 2′,7′-dichlorofluorescin diacetate (DCFH-DA; Molecular Probes), was used for the assessment of intracellular reactive oxygen species (ROS) formation.[20] This assay is widely used as a reliable method for the measurement of intracellular ROS such as hydrogen peroxide (H_2O_2), hydroxyl radicals (OH·), and hydroperoxides (ROOH). Fluorescence images (excitation at 490 nm and emission at 530 nm) were acquired with a microscope (LSM 510 Carl Zeiss).

Ca^{2+} Transient and Cell Shortening in Dog Myocytes

Myocyte shortening and intracellular calcium were measured as described previously.[11] In brief, myocytes were incubated with 1 μmol/L fura 2-AM, 0.0045% Pluronic F-127 (Sigma), and 0.1% dimethyl sulfoxide for 30 minutes, then washed twice with HEPES

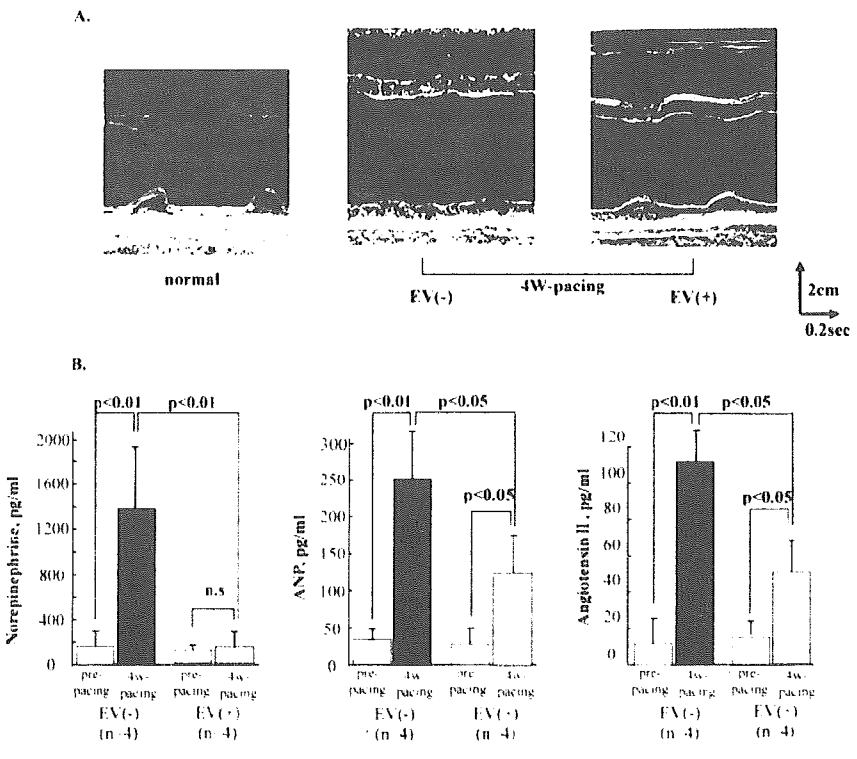

Figure 1. Effects of edaravone on cardiac function and neurohormonal factors. A, Representative M-mode echocardiogram. Note that both LV end-diastolic and LV end-systolic diameters were smaller in edaravone-treated dog than in edaravone-untreated dog. B, Plasma norepinephrine, angiotensin II, and atrial natriuretic peptide (ANP) levels before and after RV pacing for 4 weeks with or without edaravone treatment. EV(−) indicates edaravone-untreated 4-week paced group; EV(+), edaravone-treated 4-week paced group.

buffer containing (in mmol/L) NaCl 126, KCl 4.4, $MgCl_2$ 1.0, $CaCl_2$ 1.08, HEPES 24, glucose 11, NaOH 13, and probenecid 0.5 (pH 7.4). Cells were stimulated by a field electric stimulator (IonOptix) at 1.0 Hz. A dual-excitation spectrofluorometer was used to record fluorescence emissions (505 nm) elicited from exciting wavelengths at 340 and 380 nm. The intracellular calcium was monitored as the ratio of fluorescence of the cell at 360 and 380 nm excitation.

Statistical Analysis

Paired *t* tests were performed for before and after comparisons of hemodynamic data. ANOVA was used to compare data groups. When we identified a significant trend by the F test, we used the Scheffé post hoc test to compare the data. For comparison of multiple measurements, repeated-measures analysis was used. Data are expressed as mean±SD. We accepted a probability value of <0.05 as statistically significant.

Results

Determination of an Appropriate Concentration of Edaravone for Long-term Administration

To determine appropriate concentrations of edaravone for long-term administration, we examined the concentration-dependent effect of edaravone on hemodynamic parameters in normal dogs. Various amounts of edaravone were administered intravenously for 3 days for each dose, starting at 0.1 mg/kg/day with gradual increments to 1.2 mg/kg/day. At a dose of >0.9 mg/kg/day, both LV pressure and the peak +dP/dt of LV pressure tended to decrease, while the dogs were kept in a conscious state. Therefore, we used a dose of 0.6 mg/kg/day for long-term administration of edaravone in this study to circumvent the acute hemodynamic effect of edaravone.

Hemodynamic and Humoral Data

In the edaravone-treated (EV+) dogs with long-term RV pacing, both systolic and diastolic functions were largely preserved, and none of these dogs developed heart failure (Table 1, Figure 1A). Plasma norepinephrine, angiotensin II, and atrial natriuretic peptide were all higher in the edaravone-untreated paced (EV−) dogs than in normal dogs (before pacing). Long-term administration of edaravone significantly reduced the levels of all of these neurohormonal factors in the paced dogs (Figure 1B). These data indicate that in the edaravone-treated dogs, there were no signs of heart failure after long-term RV pacing.

Levels of Oxidative Stress Are Elevated in Failing Hearts

To examine the extent of oxidative stress in the pacing-induced failing hearts, we determined the levels of HNE-modified protein in cardiac tissue. Positive immunohistochemical staining for HNE-modified protein was distinct in the failing cardiac myocytes (Figure 2A, HNE+, EV−). However, in the edaravone-treated paced hearts, positive immunohistochemical staining for HNE-modified protein was absent (Figure 2A, HNE+, EV+). The relative content of free thiols in the RyR2 (for definition, see Methods) was considerably reduced in the untreated failing hearts (EV−) but was normal in EV+ hearts (Figure 2B), indicating that the oxidation of the RyR2 is in fact involved in the oxidative stress in failing hearts. After treatment with the NO donor

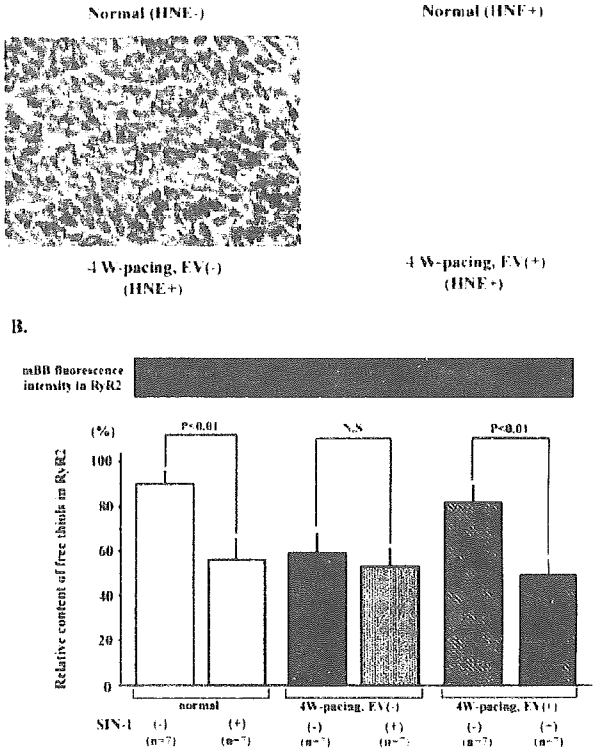

Figure 2. A, Immunohistochemical examination of HNE-modified proteins in normal and failing hearts. There is no positive staining in normal myocytes, but positive (brown) staining seen in failing hearts. B, mBB fluorescence intensity of the RyR2 (corresponding to content of free thiols) in presence or absence of 300 μmol/L SIN-1. Relative content of free thiols in RyR2 expressed as percentage of fluorescence intensity of mBB reacted with 100 μmol/L DTT (bottom).

SIN-1, which generates the NO-related species peroxynitrite ($OONO^-$),[19] approximately half of the free thiols remained unreactive (not oxidized) in all groups, consistent with the finding seen in the RyR1.[21]

Effects of Edaravone on SR Ca^{2+} Leak and Defective FKBP12.6-RyR2 Interaction in Failing Hearts

Addition of 0.3 μmol/L thapsigargin to normal SR vesicles produced little Ca^{2+} leak, whereas addition of 30 μmol/L FK506 together with 1 μmol/L thapsigargin produced a pronounced leak (Figure 3A). In contrast, in the failing (EV−) SR vesicles, the addition of thapsigargin alone produced a prominent Ca^{2+} leak, but the addition of FK506 produced no further increase (Figure 3A). In the EV+ SR vesicles, spontaneous Ca^{2+} leak was not observed, and FK506 increased Ca^{2+} leak as in the normal SR (Figure 3A).

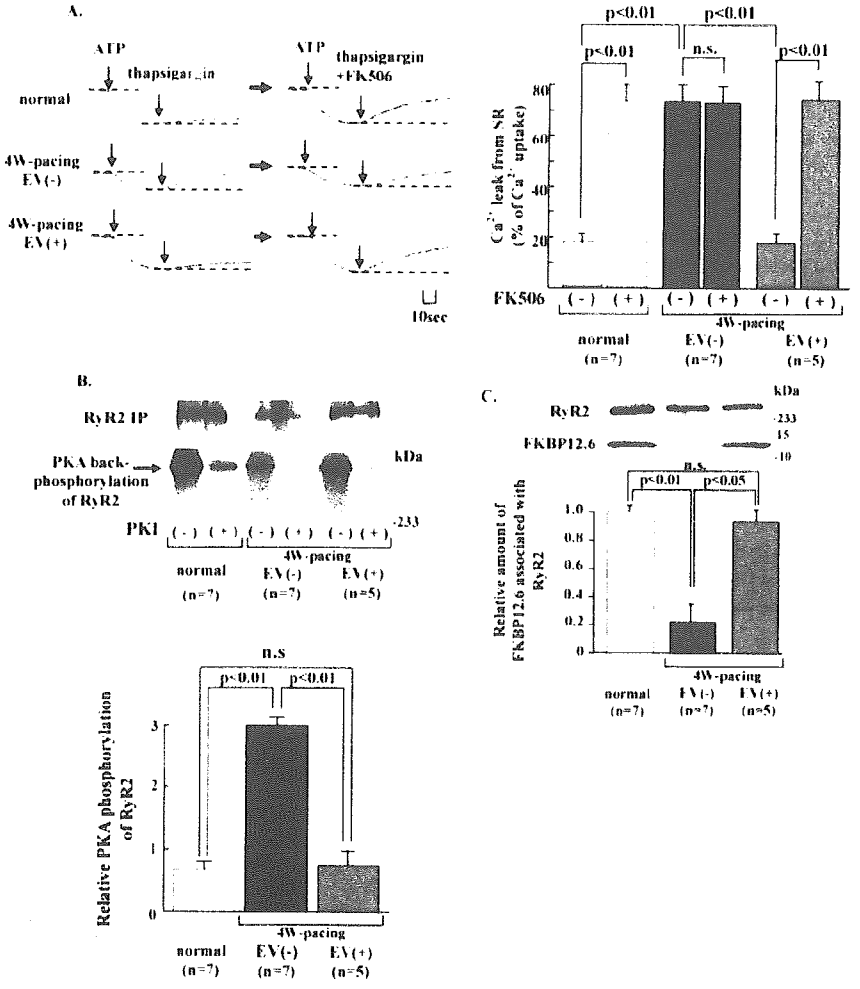

Figure 3. A, Representative time courses of Ca^{2+} uptake and ensuing Ca^{2+} leak from SR vesicles (with no cAMP; left). Note in edaravone-treated group, spontaneous Ca^{2+} leak disappeared and FK506-induced Ca^{2+} leak reappeared as in normal group. Spontaneous and FK506-induced Ca^{2+} leaks in normal, edaravone-untreated, and edaravone-treated SR vesicles are shown (right). B, PKA-mediated phosphorylation of RyR2 confirmed by back-phosphorylation. Nonspecific phosphorylation (not inhibited by PKA inhibitor [PKI]) was subtracted, and resulting value divided by amount of RyR2 protein (determined by immunoblotting and densitometry) and expressed as specific PKA-dependent γ-^{32}P incorporation ±SD. IP indicates immunoprecipitation. C, Amount of RyR2-bound FKBP12.6.

In the EV− SR vesicles, the RyR2 was PKA-hyperphosphorylated, but edaravone treatment reduced the channel phosphorylation to a level seen in the normal hearts (Figure 3B). The amount of the RyR2-associated FKBP12.6 was decreased by long-term RV pacing, but the decrease was prevented by edaravone treatment (Figure 3C).

Effects of Oxidative Stress on Ca^{2+} leak, Interdomain Interaction Within RyR2, and FKBP12.6-RyR2 Interaction

To further test the view that oxidative stress of the RyR2 is the cause of the Ca^{2+} leak, we investigated the effect of SIN-1 on the Ca^{2+} flux in normal SR. As shown in Figure 4A, 30 μmol/L SIN-1 increased the Ca^{2+} leak, and this Ca^{2+} leak was completely inhibited by 1 μmol/L JTV519, which had been found to inhibit the Ca^{2+} leak through the stabilization of the RyR2[3] via restoration of an interdomain interaction within the RyR2.[11]

To monitor the zipped and unzipped states of the interacting domains of the RyR2, we used QSY-BSA as a macromolecular quencher (Figure 4B). As in the case of our recent study with DPc10,[11] the slope of the Stern-Volmer plot, which represents K_Q or the extent of domain unzipping, was considerably increased by SIN-1 (30 μmol/L), indicating that SIN-1 in fact induced a sizable opening between the interacting domains (Figure 4B, top). The SIN-1–induced increase in the extent of fluorescence quenching was almost completely reversed by 1 μmol/L JTV519 (Figure 4B, top). This is particularly important in view of our recent finding[11] that JTV519 stabilizes the zipped configuration of the interacting domains and thus prevents Ca^{2+} leak. The extent of fluorescence quenching (K_Q) in the EV− SR vesicles was larger than in normal SR (compare Reference 11), and the addition of SIN-1 had no appreciable effect on K_Q (Figure 4B, middle). However, JTV519 reduced the K_Q in failing SR to a normal value even in the presence of SIN-1 (Figure 4B, middle). In EV+ vesicles, K_Q values were normally restored. These results suggest that domain unzipping had already occurred in failing SR partly by oxidative stress, causing Ca^{2+} leak, and that JTV519 restored the zipped state and in turn normal channel gating.

To further resolve the mechanism by which the edaravone treatment decreased the phosphorylation level of the RyR2 and inhibited FKBP12.6 dissociation from the RyR2, we investigated the effect of oxidative stress on the amount of FKBP12.6 bound with the RyR2. As seen in Figure 4C, addition of SIN-1 had no appreciable effect on the PKA phosphorylation level of the RyR2 or on FKBP12.6 binding to the RyR2 if cAMP was absent. However, in the presence of SIN-1 (30 μmol/L), the cAMP

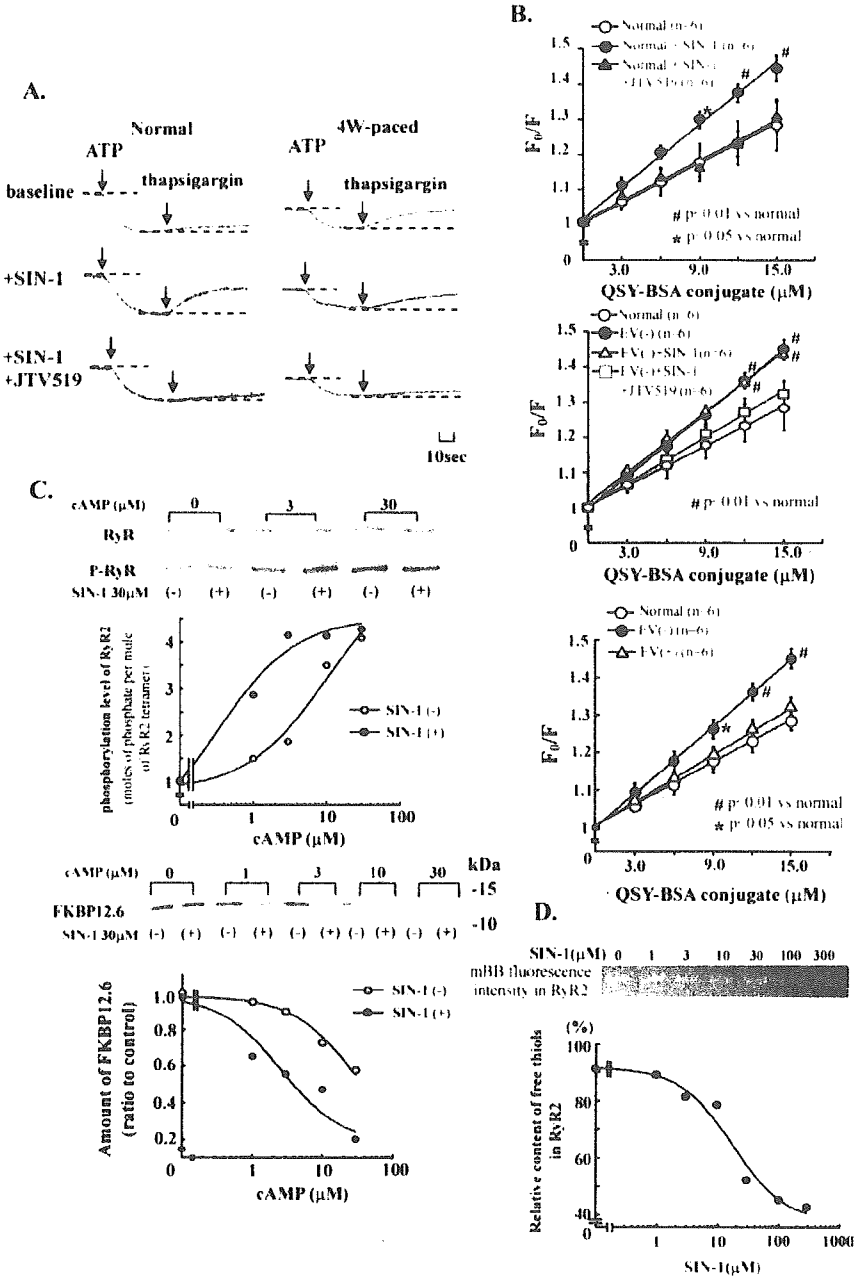

Figure 4. A, Representative time courses of Ca^{2+} uptake and Ca^{2+} leak from SR vesicles in presence of 30 μmol/L SIN-1 or 1 μmol/L JTV519 together with SIN-1 (with no cAMP). B, Stern-Volmer plots of fluorescence quenching data with QSY-BSA. Top and middle figures show effect of SIN-1 (30 μmol/L; with no cAMP) in presence or absence of 1 μmol/L JTV519 in normal and failing SR, respectively. Bottom figure shows Stern-Volmer plots of QSY-BSA fluorescence quenching data of normal, failing (edaravone-untreated), and edaravone-treated groups. C, Effect of cAMP on level PKA-dependent phosphorylation of RyR2 and FKBP12.6 dissociation in presence or absence of 30 μmol/L SIN-1. Before immunoprecipitation of RyR2, SR vesicles were mixed with SIN-1 for 30 min and centrifuged, followed by Western blotting. D, Fluorescence intensity of mBB reacted with RyR2 (corresponding to content of free thiols) after treatment with various concentrations of SIN-1. Relative content of free thiols in RyR2 was expressed as percentage of fluorescence of mBB reacted with 100 μmol/L DTT (bottom).

concentration dependence of both PKA phosphorylation of the RyR2 and FKBP12.6 dissociation was shifted toward lower concentrations of cAMP. These results suggest that domain unzipping caused by oxidative stress produces larger extents of PKA phosphorylation of the RyR2 and dissociation of FKBP12.6 from the RyR2 in the presence of cAMP at micromolar concentrations, which are presumably present in physiological conditions.

Figure 4D shows the effect of SIN-1 on the relative content of free thiols in the RyR2. SIN-1 decreased the number of free thiols of the RyR2 (ie, oxidation). Unlike edaravone, JTV519 did not rescue the oxidative stress of the RyR2 induced by SIN-1 (data not shown), indicating that the inhibition of Ca^{2+} leak by JTV519 is mediated by a mechanism independent of the RyR2 oxidation.

Effects of Edaravone on the Amount of SR Ca^{2+}-ATPase, Rate of Ca^{2+} Uptake, and Ratio of Ser16-Phosphorylated PLB and Total PLB in Failing Hearts

After rapid RV pacing for 4 weeks, both the SR Ca^{2+} uptake activity and the amount of SR Ca^{2+}-ATPase were reduced, and these changes were not observed in the EV+ group (Figure 5A, B). The levels of Ser16-phosphorylated PLB and total PLB among these groups of SR vesicles are compared in Figure 5C (top: gel picture; bottom: calculated values of relative phosphorylation). There was no difference in the level of total PLB among the 3 groups, but there was a significant decrease in the basal level of phosphorylated PLB in the failing EV− SR vesicles. In the EV+ SR vesicles, the level of phosphorylated PLB was restored back toward a normal level.

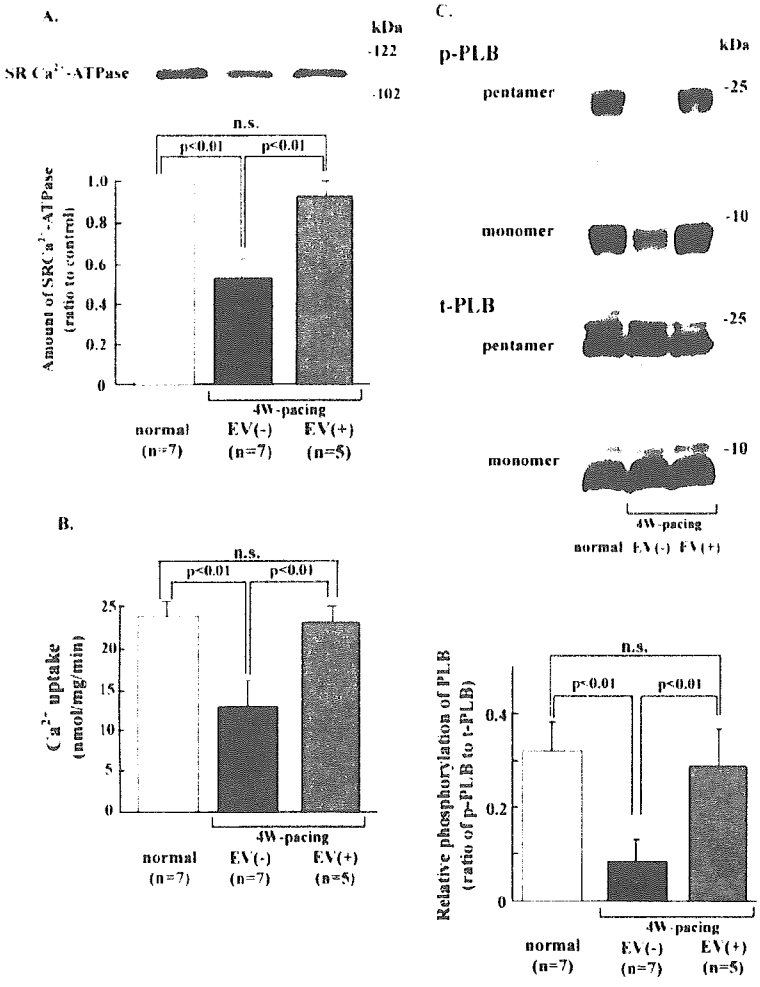

Figure 5. A, Representative Western blot of SR Ca^{2+} ATPase (top) and densitometric analysis of Western blot (bottom). B, Rate of Ca^{2+} uptake. C, Representative Western blot of Ser16-phosphorylated PLB (p-PLB) and total PLB (t-PLB; top) and densitometric analysis of Western blot (bottom). p-PLB values (sum of pentamer and monomer, in arbitrary units) normalized with respect to t-PLB values (sum of pentamer and monomer, in arbitrary units). Data presented as mean±SD.

Effects of Edaravone or JTV 519 on Ca^{2+} Transient and Cell Shortening in Normal and Failing Myocytes

We further assessed whether the adverse effects of oxidative stress on SR Ca^{2+} release function and its reversal by JTV519 seen in SR vesicles can be seen in canine myocytes as well. In normal myocytes, SIN-1 decreased the peak of Ca^{2+} transient and prolonged its duration in parallel with a reduced percent cell shortening (Figure 6A). Addition of either JTV519 (1 μmol/L) or edaravone (100 μmol/L) resulted in a significant, if not complete, restoration of both Ca^{2+} transient and cell shortening to normal levels (Figure 6A). Several reports have suggested that ROS induces intracellular Ca^{2+} overload through activation of a reversed mode of Na^{+}-Ca^{2+} exchange during reoxygenation.[22,23] Therefore, we examined the effect of the specific inhibitor of Na^{+}-Ca^{2+} exchange, SEA0400,[24] on normal myocyte function. SEA0400 (1 μmol/L) had no appreciable effect on cell shortening and peak Ca^{2+} transient at baseline. In the presence of SEA0400, SIN-1 decreased the peak of Ca^{2+} transient and prolonged its duration in parallel with a reduced percent cell shortening to an extent similar to those in the absence of SEA0400 (Figure 6A). This finding excludes the possibility that the Na^{+}-Ca^{2+} exchange may have been involved in the observed effects of SIN-1 on normal cardiomyocytes, although other radicals may influence calcium influx through reverse-mode Na^{+}-Ca^{2+} exchange activity. As shown in Figure 6B, Ca^{2+} transient and cell shortening in the myocytes isolated from pacing-induced failing dog hearts were deteriorated compared with those in normal myocytes. In the presence of isoproterenol, both Ca^{2+} transient and cell shortening were partially restored toward normal by incubation with edaravone (100 μmol/L) for 12 hours and also with JTV519 (1 μmol/L), which reverses domain unzipping.[11] Table 2 summarizes the cell shortening and Ca^{2+} transient data in normal and failing myocytes. Thus, all the data obtained from the experiments with SR vesicles and myocytes consistently support the notion that oxidative stress–induced cardiac dysfunction is induced by defective interdomain interaction in the RyR2 and that its reversal either directly by JTV519 or indirectly by edaravone restores normal cardiac function.

Figure 6C shows fluorescence images after application of the fluorescent probe of intracellular ROS, DCFH-DA (1 μmol/L), into the normal and failing cardiomyocytes. In normal cardiomyocytes, fluorescence intensity was markedly increased after addition of 100 μmol/L H_2O_2 or 30 μmol/L SIN-1, whereas it was restored to a normal level in the presence of 100 μmol/L edaravone. In failing cardiomyo-

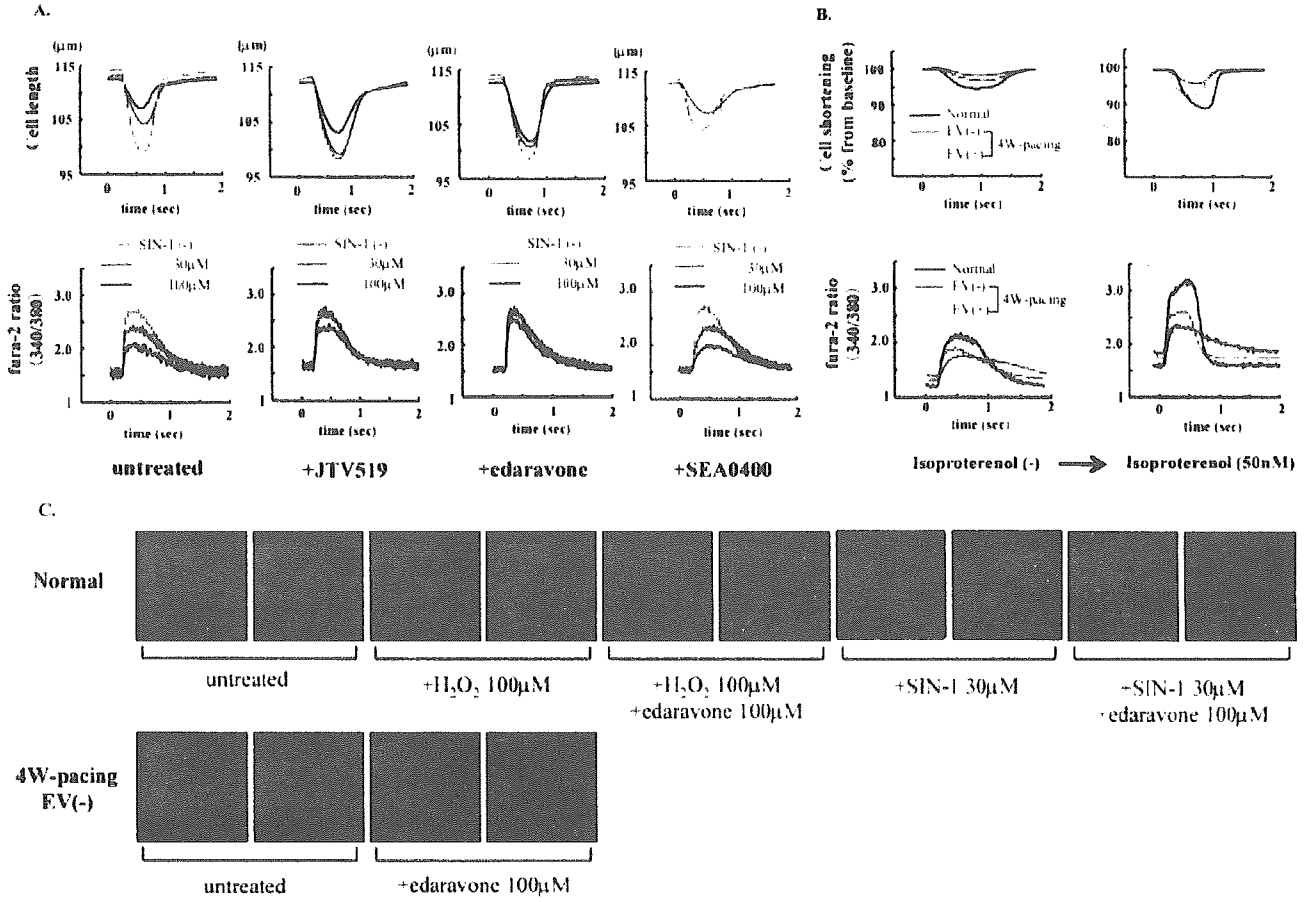

Figure 6. Cell shortening and corresponding Ca^{2+} transient in myocytes. A, Dose-dependent effect of SIN-1 in absence or presence of JTV519 (1 μmol/L), edaravone (100 μmol/L), or SEA0400 (1 μmol/L) in normal myocytes. B, Myocyte response to isoproterenol (50 nmol/L) in normal, failing (edaravone-untreated), and edaravone-treated groups. C, DCFH-DA fluorescence images in normal and failing myocytes. In normal myocytes, H_2O_2 (100 μmol/L) or SIN-1 (30 μmol/L) was added in presence or absence of edaravone (100 μmol/L). In failing myocytes, edaravone (100 μmol/L) added. Confocal microscopy clearly detects DCFH-DA fluorescence signal, indicated as green, both in failing myocytes and in normal myocytes in presence of H_2O_2 or SIN-1. Cell surface membrane fluorescently labeled as red by wheat germ agglutinin–Alexa Fluor 633 conjugate.

cytes, fluorescence intensity had already been increased to a high level, but a normal level of fluorescence intensity was restored by application of 100 μmol/L edaravone (Figure 6C) but not by 1 μmol/L JTV519 (data not shown). These findings indicate that the ROS level is indeed increased in failing myocytes, and it can be reversed by the antioxidant edaravone.

Discussion

Many reports suggested that oxidative stress caused by oxygen free radicals is in fact involved in the pathogenesis of heart failure. Several reports[25,26] have shown that there is an increased oxygen-derived free radical production in heart failure, and it can be reversed by β-blocker therapy. Recent reports also showed that the RyR is the target of ROS and that the channel activity of the RyR is regulated by oxidation or nitrosylation.[13] S-Nitrosylation of the RyR2 may have a physiological significance in the normal heart, as suggested by several reports.[27,28] However, oxidative stress often results in a deleterious loss of normal cardiac function, leading to heart failure.[13]

The most important aspect of this study is the finding that the pacing-induced heart failure and the oxidative stress–induced contractile dysfunction share at least some common causative molecular mechanisms, namely, defective interdomain interaction accompanied by a decrease in the amount of the RyR2-bound FKBP12.6 and an increase in the extent of phosphorylation. This conclusion is supported by several findings made in the present study. First, administration of the antioxidant edaravone during the course of RV pacing prevented the development of heart failure, as shown consistently in the hemodynamic, humoral, and immunohistochemical data. The treatment of the SR isolated from normal heart with the oxidant SIN-1 resulted in a considerable reduction in the content of reactive thiols in the RyR2 moiety. In the SR from failing hearts subjected to the RV pacing, the content of reactive thiols was considerably reduced, indicating that oxidative stress has occurred within the RyR2; however, the thiol content in the SR from the edaravone-treated hearts was essentially identical with that of the normal control even after RV pacing for 4 weeks. The SIN-1–induced oxidative